Journal of Scientific Computing, Vol. 31, No. 3, June 2007 (© 2006)
DOI: 10.1007/s10915-006-9108-6

An HLLC Scheme to Solve The M_1 Model of Radiative Transfer in Two Space Dimensions

Christophe Berthon,[1,2,4] **Pierre Charrier,**[1] **and Bruno Dubroca**[1,3]

Received February 7, 2006; accepted (in revised form) June 21, 2006; Published online September 10, 2006

The M_1 radiative transfer model is considered in the present work in order to simulate the radiative fields and their interactions with the matter. The model is governed by an hyperbolic system of conservation laws supplemented by relaxation source terms. Several difficulties arise when approximating the solutions of the model; namely the positiveness of the energy, the flux limitation and and the limit diffusion behavior have to be satisfied. An HLLC scheme is exhibited and it is shown to satisfy all the required properties. A particular attention is payed concerning the approximate extreme waves. These approximations are crucial to obtain an accurate scheme. The extension to the full 2D problem is proposed. It satisfies, once again, all the expected properties. Numerical experiments are proposed. They show that the considered scheme is actually less diffusive than the currently used numerical methods.

KEY WORDS: Radiative transfer; M_1 model; Asymptotic preserving; HLLC scheme; Positiveness; Flux limitation.

AMS SUBJECT CLASSIFICATIONS: Classification AMS.

1. INTRODUCTION

In many applications involving radiative transfer, solving the full radiative transfer equation is too expensive. A great effort was devoted in recent years to derive cheaper relevant models. A new alternative was introduced

[1] MAB, UMR 5466, LRC M03, Université Bordeaux I, 351 cours de la Libération, 33400 Talence, France.
[2] INRIA Futurs, projet ScAlApplix, Domaine de Voluceau-Rocquencourt, B.P. 105, 78153 Le Chesnay Cedex, France.
[3] CELIA, Université Bordeaux I, 351 cours de la Libération, 33400 Talence, France.
[4] To whom correspondence should be addressed. E-mail: Christophe.Berthon@math.u-bordeaux1.fr

by Dubroca and Feugeas [10]; namely the M_1 model. It has been used in a large literature (for instance see Turpault [25], Charrier *et al.* [9] or Ripoll [20, 21]). The M_1 model is known to preserve several crucial properties of the radiative transfer equations such as the positiveness of energy, the flux limitation, the conservation of the total energy. In addition, it recovers the asymptotic diffusion regime in the limit of large opacities (see Mihalas and Mihalas [18] or Pomraning [19]). Another important property satisfied by this model concerns 2D simulations where the shadow cone is preserved in transparent regions.

One of the main difficulties to approximate solutions is to derive numerical schemes preserving all the above properties. In [10], an HLL scheme (see Harten *et al.* [14] for details) is proposed, which satisfies the positivity of the energy and the flux limitation property. This first numerical approach is shown to fail concerning the asymptotic preserving property since it does not yield to relevant numerical approximation in the diffusion limit (for instance, see Audit *et al.* [1]). Next, in the work of [6], the authors propose a two step method based on a relaxation scheme step (see Jin and Xin [16] but also Bouchut [5] or Berthon [3] for details of the relaxation scheme in several frameworks) and a well-balanced scheme step (see Bouchut [5], Gosse and Toscani [13] and references therein), and the obtained numerical method is shown to satisfy stability properties for a simplified 1D scattering model. However, in [4], the authors establish that the scheme proposed in [6] is still too much diffusive and they detail a new relaxation numerical approach with better accuracy. From the work [4, 6], the diffusion comes with the choice of the numerical extreme wavespeeds. In [6], these wavespeeds are approximated when involving a unique constant. As announced in [4], in the present work, we propose relevant numerical approximations of each extreme wavespeed in each cell when involving a suitable approximate Riemann solver. The discrepancy with current works (see Buet *et al.* [6, 7, 8] or Gosse and Toscani [13]), stays in the structure of the approximate Riemann solver. Indeed, in the present work we consider, roughly speaking, non-symmetric approximate characteristic cone when usual approaches impose a symmetric wave cone. Such an independent consideration of the approximated wavespeed increases the accuracy of the method. Let us note from now on that the approximate characteristic cone defined by the extreme waves is of primary importance to satisfy the asymptotic preserving property. Now, if the approximate characteristic cone is too large, the numerical diffusion of the scheme increases and then the accuracy of the scheme is lost. By opposition, the scheme becomes unstable as soon as approximate characteristic cone is a too much narrow.

Arguing recent works, devoted to simplified one space dimension models, we develop an HLLC scheme for the M_1 model (see Batten *et al* [2], Bouchut [5], Toro [22] and Toro *et al.* [23] to further details concerning the

HLLC scheme in the framework of the standard gas dynamics). The structure of the approximate Riemann solver, used to define the HLLC scheme, is analysed and required stability results are established. To be more precise, we prove that the scheme satisfies the positiveness of the energy, the flux limitation property, the conservation of the total energy and the asymptotic preserving property. Next, a two space dimension extension of the scheme is proposed. To enforce the asymptotic diffusion behaviors of the 2D model, we propose to consider a relevant splitting technique of the relaxation source terms. The 2D final scheme is shown to satisfy all the required stability properties and it performs relevant numerical approximations when considering the asymptotic regimes. Moreover, thanks to the correct definition of the extreme wavespeeds, it preserves the stationary contact discontinuity which is crucial in some simulations.

The paper is organized as follows. In the next section, the M_1 model is described. The main properties satisfied by the solutions of the model are given. A special attention is payed on the asymptotic diffusion limit. In addition, the hyperbolic system is studied when giving the eigenvalues. The third section is devoted to describe an HLLC scheme to approximate the solution of the 1D model. A term by term operator splitting strategy is considered to propose a relevant method of approximation. All the properties satisfied by the exact solutions are proved to be verified by the approximate solutions. In the next section, we propose to extend the numerical scheme in the case of the 2D model. Once again, the obtained numerical scheme is shown to satisfy all the required properties. In the section five, numerical experiments are proposed. Specific 2D tests are performed to illustrate the diffuseless of the scheme. The last section is devoted to a short conclusion.

2. THE M_1 MODEL FOR RADIATIVE TRANSFER

For many applications, solving the radiative transfer equation is too expensive and cheaper moment systems, such as the M_1 model, giving accurate enough prediction of interaction of radiation and matter are prefered. To derive such systems, we take the first two moments of the radiative transfer equation (see Dubroca and Feugeas [10]), which leads to the following moment system:

$$\partial_t E + \nabla \cdot \boldsymbol{F} = c\sigma\left(aT^4 - E\right), \tag{2.1a}$$

$$\frac{1}{c}\partial_t \boldsymbol{F} + c\ \nabla \cdot \boldsymbol{P} = -\sigma\ \boldsymbol{F}, \tag{2.1b}$$

$$\partial_t(\rho\ C_v T) = -c\sigma\left(aT^4 - E\right), \tag{2.1c}$$

where E is the *radiative energy*, $\boldsymbol{F}$ *the radiative flux vector* and $\boldsymbol{P}$ the *radiative pressure tensor*. The normalized flux is written as $\boldsymbol{f}=\boldsymbol{F}/(cE)$ and $f=||\boldsymbol{f}||$ and the radiative temperature T_R is defined from the radiative energy as $E=aT_R^4$.

The radiative equations (2.1a) and (2.1b) are coupled to the material energy balance equation that writes in its simplest form (see Gentile [11] or Pomraning [19]) as Eq. (2.1c) where ρ is the matter specific density, C_v is the specific heat capacity. In the particular case of the radiativer equilibirum, we have $E(T)=aT^4$, $\boldsymbol{F}(T)=0$, $\boldsymbol{P}(T)=aT^4/3\boldsymbol{Id}$ with $a=8\pi^5k^4/15h^3c^3$ and $T_R=T$ where k is the Boltzmann constant and h the Planck constant. The moments E and $\mathbf{F}$ must verify that $E\geqslant 0$ and that $f\leqslant 1$ (flux limitation).

The radiative pressure is given by

$$\mathbf{P}=\frac{1}{2}\left((1-\chi(f))\mathbf{I}+(3\chi(f)-1)\frac{\mathbf{F}\otimes\mathbf{F}}{||\mathbf{F}||^2}\right)E, \tag{2.2}$$

where

$$\chi(f)=\frac{3+4f^2}{5+2\xi} \tag{2.3}$$

and $\xi=\sqrt{4-3f^2}$. In the present work, the model uses non normalized variables. However, the normalized model can be easily deduced when setting $c=1$ and $a=1$.

Thanks to its construction based on the minimum entropy principle, we know that this system is hyperbolic symmetrizable (see Levermore [17]). Concerning the algebra of the hyperbolic system (2.1) the Jacobian matrix set in the x-direction reads as follows

$$c\begin{pmatrix} 0 & 1 & 0 & 0 \\ \frac{(2f^2-3f_y^2)(\chi-f\chi')+f_y^2}{2f^2} & -\frac{f_xf_y^2}{2f^4}\theta+\frac{f_x\chi'}{f} & \frac{f_x^2f_y^2}{2f^4}\theta-\frac{f_y^2\chi'}{2f} & 0 \\ \frac{f_xf_y}{2f^2}(3\chi-3f\chi'-1) & \frac{f_x^2f_y}{2f^4}\theta+\frac{f_y}{2f^2}(3\chi-1) & \frac{f_xf_y^2}{4f^4}\theta+\frac{f_x}{2f^2}(3\chi-1) & 0 \\ 0 & 0 & 0 & 0 \end{pmatrix},$$

where we have set $\theta=2+3f\chi'-6\chi$. The eigenvalues of this matrix are given by

$$\begin{aligned} \lambda^{\pm}&=c\left(\frac{f_x}{\xi}\pm\frac{\sqrt{2}\sqrt{(\xi-1)(\xi+2)(2(\xi-1)(\xi+2)+3f_y^2)}}{\sqrt{3}\xi(\xi+2)}\right), \\ \lambda^0&=c\ \frac{(2-\xi)f_x}{f^2}, \quad \lambda^{\text{stationary}}=0. \end{aligned} \tag{2.4}$$

The eigenvalues of the Jacobian matrix in the y-direction are of the same form (with f_x replaced by f_y). We note that the eigenvalue $\lambda^0 = c\ \mathbf{A}_x$ where $\mathbf{A}_x$ is the x-component of the vector $\mathbf{A}$ given by,

$$\mathbf{A} = \frac{(2-\xi)\mathbf{f}}{f^2}.$$

Moreover, we can easily check that the characteristic fields associated with $\lambda^{\pm}$ are genuinely nonlinear while the characteristic field associated with λ^0 is linearly degenerate. In radiative transfer the contact discontinuities play an important role connected with the shadow effect in transparent medium as we will see in the numerical experiments.

The dimensionless eigenvalues (i.e., λ/c) of the Jacobian matrix are given on Fig. 1 as functions of f_x, respectively, for $f_y = 0$ and $f_y = \sqrt{3}/2$.

At equilibrium, i.e., for $f_x = f_y = 0$, the eigenvalues are $\lambda^{\pm} = \pm c/\sqrt{3}$, $\lambda^0 = 0$, which clearly illustrates the emission isotropy of the photons, which prevails at this regime. On the other hand, in the case of extreme non-equilibrium (for instance when f_x tends toward 1 and $f_y = 0$), both eigenvalues $\lambda^{\pm}$ tend toward $+c$, which describes that all photons move on the same direction (or that the underlying radiative intensity tends toward a Dirac which is called the free streaming regime).

For the sake of simplicity in the sequel, let us introduce the following useful notations (for the 2D M_1 model)

$$\mathcal{U} = (E, F_x/c, F_y/c)^T, \quad \mathcal{F} = (F_x, cP_{xx}, cP_{xy})^T, \qquad \mathcal{G} = (F_y, cP_{xy}, cP_{yy})^T. \tag{2.5}$$

A one dimension system can be obtained from (2.1) by assuming that all quantities are independent of y and that $F_y = 0$. Then the eigenvalues of this 3×3 system are

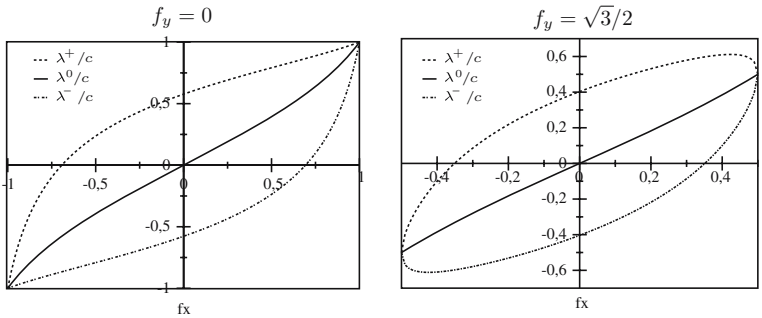

Fig. 1. Dimensionless eigenvalues of the Jacobian matrix.

$$\lambda^{\pm} = c\frac{f\sqrt{3} \pm 2(\xi - 1)}{\xi\sqrt{3}}, \quad \lambda^{\text{stationary}} = 0, \tag{2.6}$$

and coincides with the two extreme eigenvalues represented in Fig. 1. With some abuses in the 1D notations, we set

$$\mathcal{U} = (E, F/c)^T, \quad \mathcal{F} = (F, cP)^T, \tag{2.7}$$

where we have introduced $F = F_x$ in one space dimension.

It is well known that in the limit of an opaque medium (σ tends to infinity), the matter temperature can be approximated by the solution of an asymptotic model called *equilibrium diffusion equation* (see Mihalas [18] and Pomraning [19]). An important property of the M_1 system is that it recovers this equilibrium diffusion regime. Indeed, assuming that the opacity is large, we can rescale the M_1 system so that the Knudsen number ϵ appears in front of the time derivative term (long time approximation) and in the relaxation term (near equilibrium hypothesis):

$$\epsilon\partial_t E + \nabla \cdot \boldsymbol{F} = \frac{\sigma c}{\epsilon}(aT^4 - E), \tag{2.8}$$

$$\epsilon\partial_t \boldsymbol{F} + c^2\nabla \cdot \boldsymbol{P} = -\frac{\sigma c}{\epsilon}\sigma \boldsymbol{F}, \tag{2.9}$$

$$\epsilon\partial_t(\rho C_v T) = -\frac{\sigma c}{\epsilon}(aT^4 - E). \tag{2.10}$$

An asymptotic expansion around $\epsilon = 0$ gives the usual near equilibrium behavior. If we set $T = T_0 + \epsilon T_1 + \epsilon^2 T_2 + \ldots$, we get at the leading order, from Eqs. (2.8) and (2.9), $E_0 = aT_0^4$ and $\boldsymbol{F}_0 = 0$. At the next order, using Eq. (2.9) the flux can be written as $\boldsymbol{F}_1 = -c/\sigma\nabla \cdot \boldsymbol{P}_0 = -ac/3\sigma\nabla T_0^4$. Finally, summing Eqs. (2.8) and (2.10) at the following order leads to

$$\partial_t(\rho C_v T_0 + aT_0^4) - \nabla \cdot \left(\frac{4cT_0^3}{3\sigma}\nabla T_0\right) = 0, \tag{2.11}$$

which is the equilibrium diffusion equation [18].

All important properties of the M_1 system are summarized in the following result (see Dubroca and Feugeas [10])

Theorem 2.1. The radiative moment model M_1 has the following properties:

1. The radiative energy E remains positive: $E \geqslant 0$.
2. The normalized flux is limited: $f \leqslant 1$.
3. The set of admissible states $\mathcal{A} = \{\mathcal{U} = (E, \boldsymbol{F}/c) \ / \ E \geqslant 0 \ \& \ f \leq 1\}$ is a closed convex cone.

4. The system is hyperbolic and total energy $E + \rho C_v T$ is conserved:

$$\partial_t (E + \rho C_v T) + \nabla \cdot \boldsymbol{F} = 0.$$

5. The M_1 system recovers the equilibrium diffusion regime as relaxation limit for large absorption coefficient.

3. AN HLLC APPROXIMATE RIEMANN SOLVER

We propose to approximate the weak solutions of (2.1) when considering the well-known HLLC approximate Riemann solver (see Toro [22] Toro *et al.* [23], Batten *et al.* [2] or Bouchut [5] to further details). This scheme is a modification of the initial HLL method, introduced by Harten *et al.* [14], to obtain an accurate scheme. Indeed, the HLLC method exactly captures the stationary contact waves while the pioneer HLL scheme cannot satisfy such a property.

For the sake of the clarity in the presentation, the HLLC scheme is first developed in one space dimension. The extension to higher space dimension will be proposed in the next section. As a consequence, in the present section, we deal with the following hyperbolic system:

$$\begin{aligned} &\partial_t E + \partial_x F = c\sigma (aT^4 - E), \\ &\frac{1}{c} \partial_t F + \partial_x (cP) = -\sigma F, \\ &\partial_t (\rho C_v T) = -c\sigma (aT^4 - E). \end{aligned} \tag{3.1}$$

This system turns out to be hyperbolic with relaxation source terms. To develop an HLLC solver for approximating the weak solutions of (3.1), we propose a strategy of term by term operator splitting. During the first step, we evolve in time (3.1), but neglecting the matter temperature relaxation terms. The prediction is thus governed by the following system:

$$\begin{aligned} &\partial_t E + \partial_x F = 0, \\ &\frac{1}{c} \partial_t F + \partial_x (cP) = -\sigma F, \\ &\partial_t (\rho C_v T) = 0. \end{aligned} \tag{3.2}$$

The second step is devoted to introduce the matter temperature relaxation source terms $c\sigma (aT^4 - E)$. The resulting HLLC scheme will be shown to satisfy, at the discrete level, all the properties stated in Theorem 2.1.

3.1. The First Step (A Prediction)

The weak solutions of the system (3.2) are approximated involving an HLLC Riemann solver. Following the ideas introduced by Harten *et al.* [14] and extended by Toro [22] (see also Batten *et al.* [2]. Bouchut [5] and Toro *et al.* [23]), we propose to put forward an approximate Riemann solver according to system (3.2).

3.1.1. The System to be Approximated

After the recent work of [5] (and reference therein), a relevant interpretation of the relaxation source terms is proposed when introducing the variable $\Sigma(x)$ defined as follows:

$$\sigma(x) = \partial_x \Sigma(x), \tag{3.3}$$

to write (3.2) in the following form:

$$\begin{aligned} &\partial_t E + \partial_x F = 0, \\ &\frac{1}{c}\partial_t F + \partial_x (cP) = -F\partial_x \Sigma, \\ &\partial_t (\rho C_v T) = 0. \end{aligned} \tag{3.4}$$

Since Σ does not depend on the time variable, the system is completed by

$$\partial_t \Sigma = 0. \tag{3.5}$$

Now, let us note that the system (3.4)–(3.5) can be rewritten in conservation form.

Indeed, we have: $F\partial_x \Sigma = \partial_x (F\Sigma) + \partial_t (\Sigma E)$. Hence, the system (3.4)–(3.5) rewrites as follows:

$$\begin{aligned} &\partial_t E + \partial_x F = 0, \\ &\partial_t \left(\frac{1}{c} F + \Sigma E \right) + \partial_x (cP + \Sigma F) = 0, \\ &\partial_t (\rho C_v T) = 0, \\ &\partial_t \Sigma = 0. \end{aligned} \tag{3.6}$$

To shorten the notations, the system (3.6) is given in the following form:

$$\partial_t \mathcal{V} + \partial_x \mathcal{H}(\mathcal{V}) = 0, \tag{3.7}$$

where we have set

$$\mathcal{V} = \left(E, \frac{1}{c} F + \Sigma E, \rho C_v T, \Sigma \right)^T \quad \text{and} \quad \mathcal{H}(\mathcal{V}) = {}^t (F, cP + \Sigma F, 0, 0)^T .$$

An HLLC scheme is now considered to approximate the weak solutions of (3.6).

3.1.2. Definition of the HLLC Approximate Riemann Solver

To approximate the Riemann solution arising with system (3.6), we turn considering an approximate solver with the following struture (see also Fig. 2):

$$\mathcal{V}(x,t)=\begin{cases}\mathcal{V}_L, & \text{if } \frac{x}{t}<b_L,\\ \mathcal{V}_L^\star, & \text{if } b_L<\frac{x}{t}<0,\\ \mathcal{V}_R^\star, & \text{if } 0<\frac{x}{t}<b_R,\\ \mathcal{V}_R, & \text{if } \frac{x}{t}>b_R.\end{cases}$$

The wavespeeds $b_L<0<b_R$ will be estimated later according to additional stability conditions.

Let us note from now on that the initial HLLC scheme considers a middle wave with velocity $b^\star$ (see Batten *et al.* [2] or Toro [22]). In the present work, the middle wave is associated with the trivial contact wave with a vanished velocity, involved by the equations on $\rho C_v T$ and Σ. In this sense, we have imposed $b^\star=0$. Now, we have to determine the approximate states $\mathcal{V}_L^\star$ and $\mathcal{V}_R^\star$ in the star region and the corresponding flux functions $\tilde{\mathcal{H}}_L$ and $\tilde{\mathcal{H}}_R$. To access such an issue, several assumptions will be done on the choice of the linearizations. As usual, we have set

$$\mathcal{H}_L=\mathcal{H}(\mathcal{V}_L) \quad \text{and} \quad \mathcal{H}_R=\mathcal{H}(\mathcal{V}_R),$$

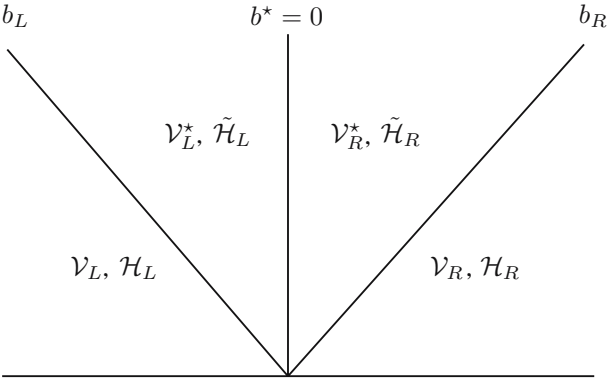

Fig. 2. Structure of the approximate Riemann solver.

but we do not impose $\tilde{\mathcal{H}}_{L,R} = \mathcal{H}(\mathcal{V}^\star_{L,R})$. To evaluate $\mathcal{V}^\star_{L,R}$ and $\tilde{\mathcal{H}}_{L,R}$, we apply the Rankine-Hugoniot conditions (see Batten *et al.* [2] and Toro [22]) across each of the waves of speed b_L and b_R:

$$\tilde{\mathcal{H}}_L - \mathcal{H}_L = b_L(\mathcal{V}^\star_L - \mathcal{V}_L), \tag{3.8}$$

$$\tilde{\mathcal{H}}_R - \mathcal{H}_R = b_R(\mathcal{V}^\star_R - \mathcal{V}_R). \tag{3.9}$$

To complete the system, we impose supplementary conditions on the approximate Riemann solver. First, let us emphasize that the quantities F and $cP + \Sigma F$ are easily shown to be continuous accross the stationary contact wave involved int he exact Riemann problem associated with (3.6). As a consequence, we propose to consider the following formulas:

$$\tilde{F}_L = \tilde{F}_R = \tilde{F}, \tag{3.10}$$

$$F^\star_L = F^\star_R = F^\star, \tag{3.11}$$

$$cP^\star_L + \tilde{\Sigma}_L \tilde{F}_L = cP^\star_R + \tilde{\Sigma}_R \tilde{F}_R, \tag{3.12}$$

$$c\tilde{P}_L + \Sigma^\star_L F^\star_L = c\tilde{P}_R + \Sigma^\star_R F^\star_R. \tag{3.13}$$

Next, we note that the exact Riemann solution of (3.6) satisfies $\Sigma(x,t) = \Sigma_L$ if $x < 0$ and $\Sigma(x,t) = \Sigma_R$ if $x > 0$. Then, we enforce the approximate Riemann solver to satisfy:

$$\tilde{\Sigma}_L = \Sigma_L \quad \text{and} \quad \tilde{\Sigma}_R = \Sigma_R. \tag{3.14}$$

Extending ideas introduced in [6], we impose the following linearization satisfied by the star-pressure:

$$P^\star_L = -\frac{b_L b_R}{c^2} E^\star_L \quad \text{and} \quad P^\star_R = -\frac{b_L b_R}{c^2} E^\star_R. \tag{3.15}$$

The HLLC approximate Riemann solver is now fully defined since he unknows $\mathcal{V}^\star_{L,R}$ and $\tilde{\mathcal{H}}_{L,R}$ are solutions of the system (3.8)–(3.15).

3.1.3. Some Notations

Before, we solve $\mathcal{V}^\star_{L,R}$ and $\tilde{\mathcal{H}}_{L,R}$, let us introduce several notations, useful in the sequel. First, we set

$$\Sigma_R - \Sigma_L = \sigma \Delta x. \tag{3.16}$$

This notation is in agreement with the exact definition of Σ given by (3.3), and it will turn out to be useful to clarify the writing of the final numerical scheme.

Next, we introduce a parameter α defined as follows:

$$\alpha = \frac{b_R - b_L}{b_R - b_L + c\sigma\,\Delta x}. \tag{3.17}$$

This parameter will play a crucial role since it will define the transport region:

$$\alpha \to 1 \quad \text{as} \quad c\sigma \to 0, \tag{3.18}$$

and the asymptotic diffusion limit

$$\alpha \to 0 \quad \text{as} \quad c\sigma \to +\infty. \tag{3.19}$$

The last notations we introduce are devoted to the standard HLL Riemann solver (see Bouchut [5], Harten *et al.* [14] and Toro [22]) when considering the system (3.6) but for an uniform vanishing σ:

$$\begin{aligned} &\partial_t E + \partial_x F = 0, \\ &\frac{1}{c}\partial_t F + \partial_x (cP) = 0, \\ &\partial_t (\rho C_v T) = 0. \end{aligned} \tag{3.20}$$

Indeed, in the case of an HLL Riemann solver, the star region is made of a constant single state defined as follows (see Toro [22] to further details, and also Fig. 2):

$$E^{\star,\mathrm{HLL}} = \frac{b_R E_R - b_L E_L - (F_R - F_L)}{b_R - b_L}, \tag{3.21}$$

$$F^{\star,\mathrm{HLL}} = \frac{b_R F_R - b_L F_L - c^2 (P_R - P_L)}{b_R - b_L}. \tag{3.22}$$

The corresponding flux functions read as follows:

$$\tilde{F}^{\mathrm{HLL}} = \frac{b_R F_L - b_L F_R - b_L b_R (E_L - E_R)}{b_R - b_L}, \tag{3.23}$$

$$\tilde{P}^{\mathrm{HLL}} = \frac{b_R P_L - b_L P_R - b_L b_R (F_L - F_R)}{b_R - b_L}. \tag{3.24}$$

Once again, let us emphasize that the notations $E^{\star,\mathrm{HLL}}$, $F^{\star,\mathrm{HLL}}$, $\tilde{F}^{\mathrm{HLL}}$, and $\tilde{P}^{\mathrm{HLL}}$ will not enter the definition of our HLLC scheme but they will short the formulas involved in the sequel of the paper.

3.1.4. Characterization of the Approximate Riemann Solver

Involving the above notations, the system (3.8)–(3.15) is solved to compute the unknowns $\mathcal{V}^\star_{L,R}$ and $\tilde{\mathcal{H}}_{L,R}$ The following statement gives this expected solution and thus the full characterization of the approximate Riemann solver is achieved:

Lemma 3.1. Let $\mathcal{V}^\star_{L,R}$ and $\tilde{\mathcal{H}}_{L,R}$ be solution of the system (3.8)–(3.15). Let us set

$$E^0_{L,R} = E_{L,R} - \frac{F_{L,R}}{b_{L,R}}. \tag{3.25}$$

Then we have

$$E^\star_{L,R} = \alpha E^{\star,\mathrm{HLL}} + (1-\alpha) E^0_{L,R}, \tag{3.26}$$
$$F^\star = \alpha F^{\star,\mathrm{HLL}}, \tag{3.27}$$
$$\Sigma^\star_{L,R} = \Sigma_{L,R}, \tag{3.28}$$
$$(\rho C_v T)^\star_{L,R} = (\rho C_v T)_{L,R} \tag{3.29}$$

and

$$\tilde{F} = \alpha \tilde{F}^{\mathrm{HLL}}, \tag{3.30}$$
$$\tilde{P}_{L,R} = \alpha \tilde{P}^{\mathrm{HLL}} + (1-\alpha)\left(P_{L,R} - \frac{b_{L,R}}{c^2} F_{L,R}\right). \tag{3.31}$$

Proof. First, from (3.8) and (3.9), we immediately deduce that

$$\Sigma^\star_L = \Sigma_L \quad \text{and} \quad \Sigma^\star_R = \Sigma_R, \tag{3.32}$$
$$(\rho C_v T)^\star_L = (\rho C_v T)_L \quad \text{and} \quad (\rho C_v T)^\star_R = (\rho C_v T)_R. \tag{3.33}$$

Next, we argue (3.8) and (3.9) to write

$$\tilde{F} - F_L = b_L(E^\star_L - E_L),$$
$$\tilde{F} - F_R = b_R(E^\star_R - E_R)$$

and then we obtain

$$(b_R - b_L)\tilde{F} - b_R F_L + b_L F_R = b_L b_R (E^\star_L - E^\star_R) - b_L b_R (E_L - E_R). \tag{3.34}$$

Moreover, from the linearization (3.15), we deduce

$$c^2 P^\star_L - c^2 P^\star_R = -b_L b_R (E^\star_L - E^\star_R). \tag{3.35}$$

When involving (3.12), we have

$$\begin{aligned} c^2 P_L^\star - c^2 P_R^\star &= c(\Sigma_R - \Sigma_L)\tilde{F}, \\ &= c\sigma \Delta x \tilde{F}, \end{aligned} \tag{3.36}$$

to obtain

$$-b_L b_R (E_L^\star - E_R^\star) = c\sigma \Delta x \tilde{F}. \tag{3.37}$$

We substitute this above identity into (3.34) to write

$$(b_R - b_L + c\sigma \Delta x)\tilde{F} = b_R F_L - b_L F_R - b_L b_R (E_L - E_R).$$

Involving (3.17) and (3.23), we obtain the expected formula (3.30) to define $\tilde{F}$.

As soon as $\tilde{F}$ is known, we can compute $\mathcal{V}_{L,R}^\star$. First, we solve $E_L^\star$ while $E_R^\star$ is obtained involving a similar computation. The Rankine–Hugoniot relation (3.8) gives:

$$\begin{aligned} b_L (E_L^\star - E_L) &= \tilde{F} - F_L, \\ &= \alpha \tilde{F}^{\mathrm{HLL}} - F_L \end{aligned}$$

to obtain

$$E_L^\star = \frac{\alpha}{b_L}(\tilde{F}^{\mathrm{HLL}} - F_L + b_L E_L) + (1-\alpha)\left(E_L - \frac{F_L}{b_L}\right).$$

In addition, from (3.21) and (3.23), we easily deduce:

$$b_L E^{\star,\mathrm{HLL}} = \tilde{F}^{\mathrm{HLL}} - F_L + b_L E_L$$

to write

$$E_L^\star = \alpha E^{\star,\mathrm{HLL}} + (1-\alpha) E_L^0. \tag{3.38}$$

Similarly, we have

$$E_R^\star = \alpha E^{\star,\mathrm{HLL}} + (1-\alpha) E_R^0. \tag{3.39}$$

The state vectors $\mathcal{V}_L^\star$ and $\mathcal{V}_R^\star$ will be solved as soon as $F^\star$ will be determined. To access such an issue, once again the relations (3.8) and (3.9) are considered to write:

$$\begin{aligned} b_L \left(\left(\frac{F^\star}{c} + \Sigma_L^\star E_L^\star \right) - \left(\frac{F_L}{c} + \Sigma_L E_L \right) \right) &= \left(c\tilde{P}_L + \tilde{\Sigma}_L \tilde{F}_L \right) - (cP_L + \Sigma_L F_L), \\ b_R \left(\left(\frac{F^\star}{c} + \Sigma_R^\star E_R^\star \right) - \left(\frac{F_R}{c} + \Sigma_R E_R \right) \right) &= \left(c\tilde{P}_R + \tilde{\Sigma}_R \tilde{F}_R \right) - (cP_R + \Sigma_R F_R). \end{aligned}$$

Involving (3.11), (3.15) and (3.28), we rewrite these relations as follows:

$$\begin{aligned}\frac{b_L}{c}(F^\star - F_L) + b_L\Sigma_L(E_L^\star - E_L) &= c(\tilde{P}_L - P_L) + \Sigma_L(\tilde{F} - F_L),\\ \frac{b_R}{c}(F^\star - F_R) + b_R\Sigma_R(E_R^\star - E_R) &= c(\tilde{P}_R - P_R) + \Sigma_R(\tilde{F} - F_R).\end{aligned} \tag{3.40}$$

Since

$$\begin{aligned}b_L(E_L^\star - E_L) &= \tilde{F} - F_L,\\ b_R(E_R^\star - E_R) &= \tilde{F} - F_R,\end{aligned} \tag{3.41}$$

we deduce from (3.40) the following identity:

$$(b_R - b_L)F^\star = c^2(\tilde{P}_R - \tilde{P}_L) - c^2(P_R - P_L) + b_R F_R - b_L F_R. \tag{3.42}$$

We involve (3.13) to write

$$c^2(\tilde{P}_R - \tilde{P}_R) = -c\sigma\,\Delta x F^\star$$

and then we obtain

$$(b_R - b_L + c\sigma\,\Delta x)F^\star = b_R F_R - b_L F_L - c^2(P_R - P_L).$$

From (3.22), we obtain the Eq. (3.27) to define $F^\star$, and the computations to estimate $\mathcal{V}_L^\star$ and $\mathcal{V}_R^\star$ are achieved.

Now, to complete the determination of $\tilde{\mathcal{H}}_L$ and $\tilde{\mathcal{H}}_R$, we have just to compute $\tilde{P}_L$ and $\tilde{P}_R$. We plug (3.41) into (3.40) to write

$$\begin{aligned}\tilde{P}_L &= P_L + \frac{b_L}{c^2}(F^\star - F_L),\\ \tilde{P}_R &= P_R + \frac{b_R}{c^2}(F^\star - F_R).\end{aligned}$$

Involving (3.24), we immediately obtain the expected identity (3.31) and the proof is thus completed. □

3.1.5. Main Properties of the Approximate Riemann Solver

To achieve the analysis of the star region, introduced in the approximate Riemann solver (see Fig. 2), we exhibit relevant conditions to enforce stability properties. With the notations introduced in (2.7), we define

$$\mathcal{U}_{L,R}^\star = \begin{pmatrix} E_{L,R}^\star \\ F^\star/c \end{pmatrix}.$$

We have to enforce that the approximate Riemann solver satisfies $\mathcal{U}^\star_{L,R} \in \mathcal{A}$ when $\mathcal{A}$, defined in Theorem 2.1, is the set of the admissible states.

Now, involving the definition of $E^\star_{L,R}$, given by (3.26), and $F^\star$, given by (3.27), we can write

$$\mathcal{U}^\star_{L,R} = \alpha \mathcal{U}^{\star,\mathrm{HLL}} + (1-\alpha)\mathcal{U}^0_{L,R},$$

where

$$\mathcal{U}^{\star,\mathrm{HLL}} = \begin{pmatrix} E^{\star,\mathrm{HLL}} \\ F^{\star,\mathrm{HLL}}/c \end{pmatrix} \quad \text{and} \quad \mathcal{U}^0_{L,R} = \begin{pmatrix} E^0_{L,R} \\ 0 \end{pmatrix}.$$

Since α, defined by (3.17), belongs to $[0,1]$, and since $\mathcal{A}$ is a convex set, we have just to establish that $\mathcal{U}^{\star,\mathrm{HLL}}$ and $\mathcal{U}^0_{L,R}$ belong to $\mathcal{A}$ in order to enforce $\mathcal{U}^\star_{L,R} \in \mathcal{A}$. In the following result, as long as the velocities b_L and b_R satisfy relevant conditions, we show that $\mathcal{U}^\star_{L,R}$ are in $\mathcal{A}$:

Lemma 3.2. Let us define

$$f_L = \frac{F_L}{cE_L} \quad \text{and} \quad f_R = \frac{F_R}{cE_R}. \tag{3.43}$$

Assume

$$b_L \leqslant \min\left(0, cf_L, c\frac{f_L-\chi_L}{1-f_L}, c\frac{f_L+\chi_L}{1+f_L}\right), \tag{3.44}$$

$$b_R \geqslant \max\left(0, cf_R, c\frac{f_R-\chi_R}{1-f_R}, c\frac{f_R+\chi_R}{1+f_R}\right), \tag{3.45}$$

where $\chi_{L,R} = \chi(f_{L,R})$ with the function χ defined by (2.3). Then $\mathcal{U}^{\star,\mathrm{HLL}}_{L,R}$ and $\mathcal{U}^0_{L,R}$ are in $\mathcal{A}$. As a consequence, $\mathcal{U}^\star_{L,R} \in \mathcal{A}$.

Proof. To obtain $\mathcal{U}^0_{L,R}$ in $\mathcal{A}$, we have just to enforce:

$$E^0_L = E_L - \frac{F_L}{b_L} \geqslant 0 \quad \text{and} \quad E^0_R = E_R - \frac{F_R}{b_R} \geqslant 0.$$

these conditions are easily see to be verified as long as (3.44) and (3.45) are satisfied. Concerning $\mathcal{U}^{\star,\mathrm{HLL}}$, we show that

$$E^{\star,\mathrm{HLL}} > 0 \quad \text{and} \quad -cE^{\star,\mathrm{HLL}} < F^{\star,\mathrm{HLL}} < cE^{\star,\mathrm{HLL}},$$

under the conditions (3.44) and (3.45). First, we write

$$E^{\star,\mathrm{HLL}} = \frac{b_R}{b_R - b_L}E^0_R + \frac{-b_L}{b_R - b_L}E^0_L.$$

Since $E^0_{L,R} > 0$, we immediately deduce that $E^{\star,\mathrm{HLL}} > 0$.

Now, concerning the flux limitation, we rewrite the condition $F^{\star,\mathrm{HLL}} < cE^{\star,\mathrm{HLL}}$ in the following form:

$$\left(b_R\left(F_R-\frac{c^2}{b_R}P_R\right)-cb_RE_R+cF_R\right)$$
$$-\left(b_L\left(F_L-\frac{c^2}{b_L}P_L\right)-cb_LE_L+cF_L\right)<0.$$

It is thus clear that the expected inequality $F^{\star,\mathrm{HLL}} < cE^{\star,\mathrm{HLL}}$ holds as soon as we have

$$b_R\left(F_R-\tfrac{c^2}{b_R}P_R\right)-cb_RE_R+cF_R<0,$$
$$b_L\left(F_L-\tfrac{c^2}{b_L}P_L\right)-cb_LE_L+cF_L>0.$$

Involving (3.43) and (2.2), we rewrite the two above inequalities in the following form:

$$b_R>c\frac{f_R-\chi_R}{1-f_R}\quad\text{and}\quad b_L<c\frac{f_L-\chi_L}{1-f_L}.$$

Arguing a similar computation, we ensure that the inequality $F^{\star,\mathrm{HLL}} > -cE^{\star,\mathrm{HLL}}$ holds as long as we have

$$b_R>c\frac{f_R+\chi_R}{1+f_R}\quad\text{and}\quad b_L<c\frac{f_L+\chi_L}{1+f_L}.$$

The proof is thus achieved. □

3.1.6. The HLLC Scheme

The above approximate Riemann solver is used to propose a relevant numerical scheme for approximating the weak solutions of (3.4). We consider a structured mesh defined by the cells $I_i=[x_{i-\frac{1}{2}},x_{i+\frac{1}{2}})$ with

$$x_{i+\frac{1}{2}}=x_i+\frac{\Delta x}{2},\qquad i\in\mathbb{Z},$$

where Δx is the spatial cell width. Under the CFL like condition:

$$\frac{\Delta t}{\Delta x}\max_{i\in\mathbb{Z}}\left(|b_L^{i+\frac{1}{2}}|,b_R^{i-\frac{1}{2}}\right)\leqslant\frac{1}{2},\tag{3.46}$$

we set, at each cell interface $x_{i+\frac{1}{2}}$, the approximate Riemann solver where $\mathcal{V}_L$ and $\mathcal{V}_R$ are substituted by $\mathcal{V}_i^n$ and $\mathcal{V}_{i+1}^n$.

The CFL condition ensures that all the Riemann solvers do not interact (see Fig. 3) where the two extreme wavespeeds are estimated involving the exact eigenvalues (2.6). After the work of Batten *et al.* [2] (see also Toro [22], Toro *et al.* [23] and Bouchut [5]), we propose to consider:

$$b_L^{i+\frac{1}{2}} \leqslant \min\left(0, cf_i^n, c\frac{f_i^n - \chi_i^n}{1 - f_i^n}, c\frac{f_i^n + \chi_i^n}{1 + f_i^n}, \lambda^-(\mathcal{U}_i^n)\right), \tag{3.47}$$

$$b_R^{i-\frac{1}{2}} \geqslant \max\left(0, cf_i^n, c\frac{f_i^n - \chi_i^n}{1 - f_i^n}, c\frac{f_i^n + \chi_i^n}{1 + f_i^n}, \lambda^+(\mathcal{U}_i^n)\right) \tag{3.48}$$

with

$$f_i^n = \frac{F_i^n}{cE_i^n} \quad \text{and} \quad \chi_i^n = \chi(f_i^n).$$

We set $\mathcal{V}^h(x, t^n + \Delta t)$ the approximate solution at time $t^n + \Delta t$, made of the juxtaposition of the non-interacting approximate Riemann solvers.

Next, the projection of these solutions on the piecewise constant functions gives:

$$\begin{pmatrix} E_i^{n+1} \\ F_i^{n+1}/c \\ (\rho C_v T)_i^{n+1} \end{pmatrix} = \frac{1}{\Delta x} \int_{x_{i-\frac{1}{2}}}^{x_{i+\frac{1}{2}}} \begin{pmatrix} E^h(x, t^n + \Delta t) \\ F^h(x, t^n + \Delta t)/c \\ (\rho C_v T)^h(x, t^n + \Delta t) \end{pmatrix} dx. \tag{3.49}$$

After an usual and easy computation, we obtain

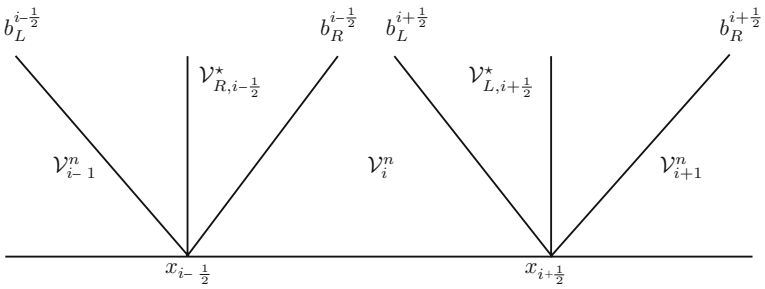

Fig. 3. HLLC scheme: Stucture of the approximate Riemann solver set on a cell $(x_{i-\frac{1}{2}}, x_{i+\frac{1}{2}})$.

$$E_i^{n+1} = E_i^n - \frac{\Delta t}{\Delta x}\left(\alpha_{i+\frac{1}{2}}\tilde{F}^{HLL}_{i+\frac{1}{2}} - \alpha_{i-\frac{1}{2}}\tilde{F}^{\mathrm{HLL}}_{i-\frac{1}{2}}\right), \tag{3.50a}$$

$$F_i^{n+1} = F_i^n - \frac{\Delta t}{\Delta x}c^2\left(\alpha_{i+\frac{1}{2}}\tilde{P}^{\mathrm{HLL}}_{i+\frac{1}{2}} - \alpha_{i-\frac{1}{2}}\tilde{P}^{\mathrm{HLL}}_{i-\frac{1}{2}} + (\alpha_{i-\frac{1}{2}} - \alpha_{i+\frac{1}{2}})P_i^n\right) + \frac{\Delta t}{\Delta x}\left((1-\alpha_{i+\frac{1}{2}})b_L^{i+\frac{1}{2}} - (1-\alpha_{i-\frac{1}{2}})b_R^{i-\frac{1}{2}}\right)F_i^n, \tag{3.50b}$$

$$(\rho C_v T)_i^{n+1} = (\rho C_v T)_i^n \tag{3.50c}$$

At this level of the scheme, we have proposed a predictor step which will be seen to preserve the positiveness of the energy E_i^{n+1} and the flux limitation (see Sect. 3.3).

3.2. The Second Step (A Correction)

The above numerical scheme (3.50) must be corrected to propose a suitable discrete form of the matter temperature relaxation source terms $c\sigma(aT^4 - E)$. To access such an issue, we propose to modify the star region states, $\mathcal{V}^\star_{L,R}$, introduced in the approximate Riemann solver (see Fig. 2), according to the relaxation source terms. Put in other words, the state vectors $\mathcal{V}^\star_{L,R}$ and the corresponding flux function $\tilde{\mathcal{H}}_{L,R}$ must be corrected to satisfy a suitable approximation of

$$\begin{aligned}
&\partial_t E = c\sigma(aT^4 - E),\\
&\partial_t F = 0,\\
&\partial_t(\rho C_v T) = -c\sigma(aT^4 - E).
\end{aligned}$$

The corrected results will be denoted $\mathcal{V}^{\star,\mathrm{HLLC}}_{L,R}$ and $\tilde{\mathcal{H}}^{\mathrm{HLLC}}_{L,R}$. They will be defined as follows:

$$\begin{aligned}
&E^{\star,\mathrm{HLLC}}_{L,R} - E^\star_{L,R} = (1-\alpha)\left(a\left(T^{\star,\mathrm{HLLC}}_{L,R}\right)^4 - E^0_{L,R}\right),\\
&F^{\star,\mathrm{HLLC}}_{L,R} - F^\star = 0,\\
&\rho C_v\left(T^{\star,\mathrm{HLLC}}_{L,R} - T^\star_{L,R}\right) = -(1-\alpha)\left(a\left(T^{\star,\mathrm{HLLC}}_{L,R}\right)^4 - E^0_{L,R}\right),
\end{aligned}$$

where α is defined by (3.17), $E^\star_{L,R}$ is given by (3.26), $F^\star$ is given by (3.27) and $E^0_{L,R}$ is given by (3.25). We easily deduce the following corrected approximation for E and F:

$$E^{\star,\mathrm{HLLC}}_{L,R} = \alpha E^{\star,\mathrm{HLL}} + (1-\alpha)a\left(T^{\star,\mathrm{HLLC}}_{L,R}\right)^4, \tag{3.51}$$

$$F^{\star,\mathrm{HLLC}}_{L,R} = \alpha F^{\star,\mathrm{HLL}}. \tag{3.52}$$

Arguing the definition (2.7), we write for short

$$\mathcal{U}_{L,R}^{\star,\mathrm{HLLC}} = \alpha \mathcal{U}^{\star,\mathrm{HLL}} + (1-\alpha)\mathcal{U}_{L,R}^{a}, \tag{3.53}$$

where $\mathcal{U}_{L,R}^{a}$ corresponds to the asymptotic state and it is defined as follows:

$$\mathcal{U}_{L,R}^{a} = \begin{pmatrix} a\left(T_{L,R}^{\star,\mathrm{HLLC}}\right)^4 \\ 0 \end{pmatrix}, \tag{3.54}$$

with $T_{L,R}^{\star,\mathrm{HLLC}}$ defined in the following result:

Lemma 3.3. The matter temperature $T_{L,R}^{\star,\mathrm{HLLC}}$ is the unique solution of the following equation:

$$\rho C_v T_{L,R}^{\star,\mathrm{HLLC}} + (1-\alpha)a(T_{L,R}^{\star,\mathrm{HLLC}})^4 = \rho C_v T_{L,R} + (1-\alpha)E_{L,R}^{0}. \tag{3.55}$$

In addition, $T_{L,R}^{\star,\mathrm{HLLC}}$ is positive.

The proof of this result turns out to be obvious and it is omitted. Now, we can establish that the corrected states $\mathcal{U}_{L,R}^{\star,\mathrm{HLLC}}$ belong to $\mathcal{A}$.

Lemma 3.4. Let us consider the assumptions stated in Lemma 3.2. Then, $\mathcal{U}_{L,R}^{\star,\mathrm{HLLC}}$, defined by (3.53), belongs to $\mathcal{A}$.

Proof. From Lemma 3.2, we have $\mathcal{U}^{\star,\mathrm{HLL}} \in \mathcal{A}$. In addition, after the positiveness of $T_{L,R}^{\star,\mathrm{HLLC}}$, we easily deduce that

$$\begin{pmatrix} a\left(T_{L,R}^{\star,\mathrm{HLLC}}\right)^4 \\ 0 \end{pmatrix} \in \mathcal{A}.$$

Now, applying the convex property of $\mathcal{A}$, we immediately obtain the expected result. □

To conclude the determination of the corrected states, $\mathcal{V}_{L,R}^{\star,\mathrm{HLLC}}$, we specify the asymptotic behavior of the approximate Riemann solver. Indeed, let us assume that $c\sigma$ goes to zero (or equivalently, α tends to 1). In this case, we typically enter the regime of pure transport equations. From (3.51), (3.52) and (3.55), we have for such a limit:

$$\begin{aligned} E_{L,R}^{\star,\mathrm{HLLC}} &\to E^{\star,\mathrm{HLL}}, \\ F_{L,R}^{\star,\mathrm{HLLC}} &\to F^{\star,\mathrm{HLL}}, \\ T_{L,R}^{\star,\mathrm{HLLC}} &\to T_{L,R}. \end{aligned}$$

As expected, the approximate Riemann solver coincides with the standard Riemann solver involved when considering an HLLC scheme to approximate solutions of (3.20).

Now, we turn considering the asymptotic behavior as long as $c\sigma$ goes to infinity, or equivalently assume that α tends to 0. In this case, we obtain the following limit:

$$\begin{aligned} E_{L,R}^{\star,\mathrm{HLLC}} &\to a\left(T_{L,R}^{\star,\mathrm{HLLC}}\right)^4, \\ F_{L,R}^{\star,\mathrm{HLLC}} &\to 0 \end{aligned}$$

to coincide with the asymptotic diffusion regime.

To complete the determination of the star region, we have to solve the resulting flux function $\tilde{\mathcal{H}}_{L,R}^{\mathrm{HLLC}}$. It will be done as soon as $\tilde{F}_{L,R}^{\mathrm{HLLC}}$ and $\tilde{P}_{L,R}^{\mathrm{HLLC}}$ should be evaluated. To access such an issue, once again, we consider the Rankine–Hugoniot relations (3.8) and (3.9). First, we have

$$\tilde{F}_{L,R}^{\mathrm{HLLC}} = F_{L,R} + b_{L,R}\left(E_{L,R}^{\star,\mathrm{HLLC}} - E_{L,R}\right).$$

Involving (3.51), we obtain

$$\tilde{F}_{L,R}^{\mathrm{HLLC}} = \alpha\tilde{F}^{\mathrm{HLL}} + (1-\alpha)b_{L,R}\left(a\left(T_{L,R}^{\star,\mathrm{HLLC}}\right)^4 - E_{L,R}^0\right). \tag{3.56}$$

Similarly, from (3.8) and (3.9), we deduce

$$c^2\tilde{P}_{L,R}^{\mathrm{HLLC}} = c^2 P_{L,R} + b_{L,R}\left(F_{L,R}^{\star,\mathrm{HLLC}} - F_{L,R}\right),$$

to write when considering (3.52):

$$c^2\tilde{P}_{L,R}^{\mathrm{HLLC}} = \alpha c^2\tilde{P}^{\mathrm{HLL}} + (1-\alpha)\left(c^2 P_{L,R} - b_{L,R}F_{L,R}\right). \tag{3.57}$$

To conclude the description of the approximate Riemann solver, let us note that the corresponding flux function $\tilde{\mathcal{F}}_{L,R}^{\mathrm{HLLC}}$, associated with $\mathcal{U}_{L,R}^{\star,\mathrm{HLLC}}$, reads as follows:

$$\tilde{\mathcal{F}}_{L,R}^{\mathrm{HLLC}} = \alpha\tilde{\mathcal{F}}^{\mathrm{HLL}} + (1-\alpha)\mathcal{S}_{L,R}^a, \tag{3.58}$$

where $\mathcal{S}_{L,R}^a$ is given by

$$\mathcal{S}_{L,R}^a = b_{L,R}\left(\mathcal{U}_{L,R}^a - \mathcal{U}_{L,R}^0\right), \tag{3.59}$$

$$\mathcal{U}_{L,R}^0 = \mathcal{U}_{L,R} - \frac{1}{b_{L,R}}\mathcal{F}_{L,R}. \tag{3.60}$$

Of course, in a practical point of view, the equivalent formulas (3.56) and (3.57) are preferred. In fact, (3.58) and (3.59) will play a useful role for the 2D extension of the scheme. In addition, we note from now on that $\tilde{\mathcal{F}}^{\mathrm{HLL}}$ will participate to the discretization of the transport part while the discrete form of the relaxation source terms inherit from $\mathcal{S}^a_{L,R}$. We add that the jump relations applied to the matter temperature reads

$$\begin{aligned}\mathcal{S}^T_{L,R} &= b_{L,R}\rho C_v\left(T^{\star,\mathrm{HLLC}}_{L,R} - T_{L,R}\right),\\ &= -b_{L,R}(1-\alpha)\left(a\left(T^{\star,\mathrm{HLLC}}_{L,R}\right)^4 - E^0_{L,R}\right).\end{aligned} \tag{3.61}$$

Actually, this relation play a central role in the discrete form of source terms involved in the matter temperature evolution equation (see Eq. (3.62)).

Now, involving the corrected approximate Riemann solver, defined by (3.51), (3.52) and (3.55), we describe the expected HLLC scheme to approximate the solutions of system (3.1). We consider the same strategy as used in the prediction step (see Fig. 4).

We adopt the CFL restriction (3.46). The approximate Riemann solver, at time $t^n + \Delta t$, is projected on the piecewise constant functions following (3.49). After the computations, the achieved scheme reads as follows:

$$\begin{aligned}E_i^{n+1} = E_i^n &- \frac{\Delta t}{\Delta x}\left(\alpha_{i+\frac{1}{2}}\tilde{F}^{\mathrm{HLL}}_{i+\frac{1}{2}} - \alpha_{i-\frac{1}{2}}\tilde{F}^{\mathrm{HLL}}_{i-\frac{1}{2}}\right)\\ &- \frac{\Delta t}{\Delta x}\left(\left(1-\alpha_{i+\frac{1}{2}}\right)b_L^{i+\frac{1}{2}}\left(a\left(T^{\star,\mathrm{HLLC}}_{L,i+\frac{1}{2}}\right)^4 - \left(E_i^n - \frac{F_i^n}{b_L^{i+\frac{1}{2}}}\right)\right)\right.\\ &\left.- \left(1-\alpha_{i-\frac{1}{2}}\right)b_R^{i-\frac{1}{2}}\left(a\left(T^{\star,\mathrm{HLLC}}_{R,i-\frac{1}{2}}\right)^4 - \left(E_i^n - \frac{F_i^n}{b_R^{i-\frac{1}{2}}}\right)\right)\right),\end{aligned} \tag{3.62a}$$

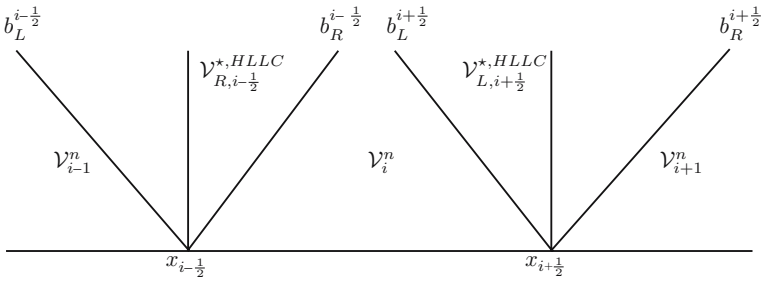

Fig. 4. Structure of the approximate Riemann solver for the corrected HLLC scheme.

$$F_i^{n+1} = F_i^n - \frac{\Delta t}{\Delta x} c^2 \left(\alpha_{i+\frac{1}{2}} \tilde{P}^{\mathrm{HLL}}_{i+\frac{1}{2}} - \alpha_{i-\frac{1}{2}} \tilde{P}^{\mathrm{HLL}}_{i-\frac{1}{2}} + \left(\alpha_{i-\frac{1}{2}} - \alpha_{i+\frac{1}{2}} \right) P_i^n \right) + \frac{\Delta t}{\Delta x} \left(\left(1 - \alpha_{i+\frac{1}{2}} \right) b_L^{i+\frac{1}{2}} - \left(1 - \alpha_{i-\frac{1}{2}} \right) b_R^{i-\frac{1}{2}} \right) F_i^n, \tag{3.62b}$$

$$(\rho C_v T)_i^{n+1} = (\rho C_v T)_i^n + \frac{\Delta t}{\Delta x} \left(\left(1 - \alpha_{i+\frac{1}{2}} \right) b_L^{i+\frac{1}{2}} \left(a \left(T^{\star,\mathrm{HLLC}}_{L,i+\frac{1}{2}} \right)^4 - \left(E_i^n - \frac{F_i^n}{b_L^{i+\frac{1}{2}}} \right) \right) - \left(1 - \alpha_{i-\frac{1}{2}} \right) b_R^{i-\frac{1}{2}} \left(a \left(T^{\star,\mathrm{HLLC}}_{R,i-\frac{1}{2}} \right)^4 - \left(E_i^n - \frac{F_i^n}{b_R^{i-\frac{1}{2}}} \right) \right) \right). \tag{3.62c}$$

3.3. The Main Properties

We turn establishing the main properties satisfied by the approximate solutions. These properties will emphasize that the scheme is relevant. We give the discrete version of Theorem 2.1. In a first result, the positiveness of the radiative energy, the flux limitation and the conservation of the total energy are proved. Next, a second statement shows that the considered scheme satisfies the expected asymptotic limit as long as the parameter $c\sigma$ goes to infinity.

Theorem 3.5. Let $\mathcal{U}_i^n$ be in $\mathcal{A}$ and T_i^n be positive. Assume the CFL restriction (3.46) where the wavespeeds $b_L^{i+\frac{1}{2}}$ and $b_R^{i-\frac{1}{2}}$ are given by (3.47)–(3.48). The updated approximate solution $\mathcal{U}_i^{n+1}$, defined by (3.62), satisfies the following properties:

1. the radiative energy E_i^{n+1} remains positive,
2. the normalized flux is limited: $|f_i^{n+1}| \leqslant 1$,
3. the total energy $(E + \rho C_v T)_i^{n+1}$ is conserved.

Proof. The two first properties are proved when establishing that $\mathcal{U}_i^{n+1}$ belongs to $\mathcal{A}$. By definition of the scheme (3.62b), $\mathcal{U}_i^{n+1}$ is obtained after considering the projection (3.49) of the approximate Riemann solver on the piecewise constant function:

$$\mathcal{U}_i^{n+1} = \frac{1}{\Delta x} \int_{x_{i-\frac{1}{2}}}^{x_{i+\frac{1}{2}}} \mathcal{U}^h(x, t^+ \Delta t) dx,$$

$$= b_R^{i-\frac{1}{2}} \frac{\Delta t}{\Delta x} \mathcal{U}^{\star,\mathrm{HLLC}}_{R,i-\frac{1}{2}} + \left(1 - \left(b_R^{i-\frac{1}{2}} - b_L^{i+\frac{1}{2}} \right) \frac{\Delta t}{\Delta x} \right) \mathcal{U}_i^n - b_L^{i+\frac{1}{2}} \frac{\Delta t}{\Delta x} U^{\star,\mathrm{HLLC}}_{L,i+\frac{1}{2}}.$$

Under the CFL like condition (3.46), $\mathcal{U}_i^n$ is a convex sum of the states $\mathcal{U}_i^n$, $\mathcal{U}_{R,i-\frac{1}{2}}^{\star,\mathrm{HLLC}}$ and $\mathcal{U}_{L,i+\frac{1}{2}}^{\star,\mathrm{HLLC}}$. The definitions (3.47)–(3.48) allow to apply Lemma 3.4 and thus $\mathcal{U}_{R,i-\frac{1}{2}}^{\star,\mathrm{HLLC}}$ and $\mathcal{U}_{L,i+\frac{1}{2}}^{\star,\mathrm{HLLC}}$ are in $\mathcal{A}$. Since $\mathcal{U}_i^n \in \mathcal{A}$, involving the convex property of $\mathcal{A}$, we obtain $\mathcal{U}_i^{n+1} \in \mathcal{A}$.

The conservation of the total energy $(E+\rho C_v T)_i^{n+1}$ is a direct consequence of (3.62) since we have

$$(E+\rho C_v T)_i^{n+1} = (E+\rho C_v T)_i^n - \frac{\Delta t}{\Delta x}\left(\alpha_{i+\frac{1}{2}}\tilde{F}_{i+\frac{1}{2}}^{\mathrm{HLL}} - \alpha_{i-\frac{1}{2}}\tilde{F}_{i-\frac{1}{2}}^{\mathrm{HLL}}\right). \tag{3.63}$$

The proof is completed. □

We conclude the present section when establishing that the considered scheme (3.62) is asymptotic preserving. We show that the standard diffusion regime is recovered in the relaxation limit. Following the rescaling introduced into the system (2.8), we consider the Knudsen number ϵ which appears in front of the time derivative terms and in the relaxation terms. Involving such a rescaling, the scheme (3.62) rewrites as follows:

$$\begin{aligned}
&\epsilon\frac{E_i^{n+1}-E_i^n}{\Delta t} + \frac{1}{\Delta x}\left(\alpha_{i+\frac{1}{2}}\tilde{F}_{i+\frac{1}{2}}^{\mathrm{HLL}} - \alpha_{i-\frac{1}{2}}\tilde{F}_{i-\frac{1}{2}}^{\mathrm{HLL}}\right)\\
&\quad = -\left(\frac{1-\alpha_{i+\frac{1}{2}}}{\Delta x} b_L^{i+\frac{1}{2}}\left(a\left(T_{L,i+\frac{1}{2}}^{\star,\mathrm{HLLC}}\right)^4 - \left(E_i^n - \frac{F_i^n}{b_L^{i+\frac{1}{2}}}\right)\right)\right.\\
&\qquad \left. - \frac{1-\alpha_{i-\frac{1}{2}}}{\Delta x} b_R^{i-\frac{1}{2}}\left(a\left(T_{R,i-\frac{1}{2}}^{\star,\mathrm{HLLC}}\right)^4 - \left(E_i^n - \frac{F_i^n}{b_R^{i-\frac{1}{2}}}\right)\right)\right),
\end{aligned} \tag{3.64a}$$

$$\begin{aligned}
&\epsilon\frac{F_i^{n+1}-F_i^n}{\Delta t} + \frac{c^2}{\Delta x}\left(\alpha_{i+\frac{1}{2}}\tilde{P}_{i+\frac{1}{2}}^{\mathrm{HLL}} - \alpha_{i-\frac{1}{2}}\tilde{P}_{i-\frac{1}{2}}^{\mathrm{HLL}} + \left(\alpha_{i-\frac{1}{2}} - \alpha_{i+\frac{1}{2}}\right)P_i^n\right)\\
&\quad = -\left(\frac{1-\alpha_{i+\frac{1}{2}}}{\Delta x} b_L^{i+\frac{1}{2}} - \frac{1-\alpha_{i-\frac{1}{2}}}{\Delta x} b_R^{i-\frac{1}{2}}\right) F_i^n,
\end{aligned} \tag{3.64b}$$

$$\begin{aligned}
&\epsilon\frac{(\rho C_v T)_i^{n+1} - (\rho C_v T)_i^n}{\Delta t} = \frac{1-\alpha_{i+\frac{1}{2}}}{\Delta x} b_L^{i+\frac{1}{2}}\left(a\left(T_{L,i+\frac{1}{2}}^{\star,\mathrm{HLLC}}\right)^4 - \left(E_i^n - \frac{F_i^n}{b_L^{i+\frac{1}{2}}}\right)\right.\\
&\qquad \left. - \frac{1-\alpha_{i-\frac{1}{2}}}{\Delta x} b_R^{i-\frac{1}{2}}\left(a\left(T_{R,i-\frac{1}{2}}^{\star,\mathrm{HLLC}}\right)^4 - \left(E_i^n - \frac{F_i^n}{b_R^{i-\frac{1}{2}}}\right)\right)\right),
\end{aligned} \tag{3.64c}$$

where the definition of $\alpha_{i+\frac{1}{2}}$ becomes

$$\alpha_{i+\frac{1}{2}} = \frac{\epsilon\left(b_R^{i+\frac{1}{2}} - b_L^{i+\frac{1}{2}}\right)}{\epsilon\left(b_R^{i+\frac{1}{2}} - b_L^{i+\frac{1}{2}}\right) + c\sigma_{i+\frac{1}{2}}\Delta x}. \tag{3.65}$$

The behavior of the rescaled scheme in the limit of ϵ to zero is given in the following result which is nothing but the discrete Version of 5) in theorem 2.1:

Theorem 3.6. Assume the wavespeed $b_{L,R}^{i+\frac{1}{2}}$ to be given by

$$b_L^{i+\frac{1}{2}} = \min\left(0, cf_i^n, c\frac{f_i^n - \chi_i^n}{1 - f_i^n}, c\frac{f_i^n + \chi_i^n}{1 + f_i^n}, \lambda^-(\mathcal{U}_i^n)\right), \tag{3.66}$$

$$b_R^{i-\frac{1}{2}} = \max\left(0, cf_i^n, c\frac{f_i^n - \chi_i^n}{1 - f_i^n}, c\frac{f_i^n + \chi_i^n}{1 + f_i^n}, \lambda^+(\mathcal{U}_i^n)\right) \tag{3.67}$$

so that the conditions (3.47) and (3.48) are satisfied. With ϵ small, the diffusion limit of the scheme (3.64) and (3.65) is given by

$$\begin{aligned} &E_i^n = a(T_i^n)^4, \\ &F_i^n = 0, \\ &\frac{(E + \rho C_v T)_i^{n+1} - (E + \rho C_v T)_i^n}{\Delta t} \\ &\quad = \frac{c}{3\Delta x^2}\left(\frac{1}{\sigma_{i+\frac{1}{2}}}(E_{i+1}^n - E_i^n) + \frac{1}{\sigma_{i-\frac{1}{2}}}(E_{i-1}^n - E_i^n)\right). \end{aligned} \tag{3.68}$$

Proof. From (3.65), we immediately deduce that

$$\lim_{\epsilon \to 0} \alpha_{i+\frac{1}{2}} = 0.$$

Now, when considering (3.64b), we obtain the following asymptotic behavior:

$$F_i^n = 0.$$

Similarly, the relation (3.64a) rewrites

$$b_R^{i-\frac{1}{2}}\left(a\left(T_{R,i-\frac{1}{2}}^{\star,\mathrm{HLLC}}\right)^4 - E_i^n\right) - b_L^{i+\frac{1}{2}}\left(a\left(T_{L,i+\frac{1}{2}}^{\star,\mathrm{HLLC}}\right)^4 - E_i^n\right) = 0. \tag{3.69}$$

In addition, the Eq. (3.55) governing the matter temperature $T^{\star,\mathrm{HLLC}}_{L,R}$ reads in the asymptotic regime

$$\rho C_v T^{\star,\mathrm{HLLC}}_{L,R} + a\left(T^{\star,\mathrm{HLLC}}_{L,R}\right)^4 = \rho C_v T_{L,R} + E_{L,R}$$

to obtain

$$a\left(T^{\star,\mathrm{HLLC}}_{R,i-\frac{1}{2}}\right)^4 - E_i^n = \rho C_v\left(T_i^n - T^{\star,\mathrm{HLLC}}_{R,i-\frac{1}{2}}\right), \tag{3.70}$$

$$a\left(T^{\star,\mathrm{HLLC}}_{L,i+\frac{1}{2}}\right)^4 - E_i^n = \rho C_v\left(T_i^n - T^{\star,\mathrm{HLLC}}_{L,i+\frac{1}{2}}\right). \tag{3.71}$$

By solving (3.69), (3.70) and (3.71), we have

$$T^{\star,\mathrm{HLLC}}_{R,i-\frac{1}{2}} = T^{\star,\mathrm{HLLC}}_{L,i+\frac{1}{2}} = T_i^n \quad \text{and} \quad E_i^n = a(T_i^n)^4$$

The proof will be concluded when establishing the diffusion equation (3.68). First, we emphasize the behavior of the wavespeeds $b_L^{i+\frac{1}{2}}$ and $b_R^{i+\frac{1}{2}}$. Indeed, involving the definition of $b_{L,R}^{i+\frac{1}{2}}$, given by (3.66) and (3.67), and the wavespeed limitations (3.44) and (3.45), with $F_i^n = 0$ we obtain

$$b_L^{i+\frac{1}{2}} = -\frac{c}{\sqrt{3}} \quad \text{and} \quad b_R^{i+\frac{1}{2}} = \frac{c}{\sqrt{3}}. \tag{3.72}$$

Now, the standard HLL flux function $\tilde{F}^{\mathrm{HLL}}$, defined by (3.23), reads in the asymptotic regime

$$\tilde{F}^{\mathrm{HLL}}_{i+\frac{1}{2}} = -\frac{c}{2\sqrt{3}}(E_{i+1}^n - E_i^n).$$

As a consequence, (3.64a) and (3.64c) rewrite in the following form:

$$\epsilon\frac{(E+\rho C_v T)_i^{n+1} - (E+\rho C_v T)_i^n}{\Delta t} = \frac{c}{2\sqrt{3}\Delta x}\left(\alpha_{i+\frac{1}{2}}(E_{i+1}^n - E_i^n) + \alpha_{i-\frac{1}{2}}(E_{i-1}^n - E_i^n)\right). \tag{3.73}$$

Involving (3.72), the parameter $\alpha_{i+\frac{1}{2}}$ reads as follows:

$$\alpha_{i+\frac{1}{2}} = \frac{2\epsilon}{2\epsilon + \sqrt{3}\Delta x \sigma_{i+\frac{1}{2}}}.$$

Hence, from (3.73) we deduce

$$\frac{(E+\rho C_v T)_i^{n+1}-(E+\rho C_v T)_i^n}{\Delta t} = \frac{c}{2\epsilon\Delta x\sqrt{3}+3\sigma_{i+\frac{1}{2}}\Delta x^2}(E_{i+1}^n - E_i^n) + \frac{c}{2\epsilon\Delta x\sqrt{3}+3\sigma_{i-\frac{1}{2}}\Delta x^2}(E_{i-1}^n - E_i^n).$$

The expected diffusion equation (3.68) is thus obtained as soon as ϵ tends to zero. The proof is achieved. □

4. THE TWO DIMENSIONAL EXTENSION

The above HLLC scheme is now extended to the full space dimension M_1 model given by (2.1). A Cartesian grid is considered to approximate the solution. Let us note that extensions involving other grid generation methods (unstrutured Godlewsky and Raviart [12], Cartesian cut cell Ingram *et al.* [15]) can be obtained. We propose to adopt a dimensional operator splitting strategy. In a first step, we approximate the following 1D system:

$$\begin{aligned}
&\partial_t E + \partial_x F_x = \beta c\sigma(aT^4 - E),\\
&\frac{1}{c}\partial_t F_x + c\partial_x P_{xx} = -\beta\sigma F_x,\\
&\frac{1}{c}\partial_t F_y + c\partial_x P_{xy} = -\beta\sigma F_y,\\
&\partial_t(\rho C_v T) = -\beta c\sigma(aT^4 - E),
\end{aligned} \tag{4.1}$$

while, into the second step, the following system will be considered:

$$\begin{aligned}
&\partial_t E + \partial_y F_y = (1-\beta)c\sigma(aT^4 - E),\\
&\frac{1}{c}\partial_t F_x + c\partial_y P_{xy} = -(1-\beta)\sigma F_x,\\
&\frac{1}{c}\partial_t F_y + c\partial_y P_{yy} = -(1-\beta)\sigma F_y,\\
&\partial_t(\rho C_v T) = -(1-\beta)c\sigma(aT^4 - E),
\end{aligned} \tag{4.2}$$

where β is a given parameter in $[0, 1]$. The main idea of the present splitting lies on the choice of the source terms. Indeed, the relaxation terms are split over each step involving a parameter β. To ensure consistancy of the splitting, this parameter β will belong to $[0, 1]$. A relevant choice will be proposed in the next section devoted to the numerical experiments.

In the present section, we will just describe the first step since the second one is analogous reversing the role played by each dimension component (F_x, P_{xx}, P_{xy}) and (F_y, P_{xy}, P_{yy}). Following the ideas introduced to

approximate the 1D model, we propose to consider an approximate Riemann solver and thus define an HLLC type scheme. One of the main difference with the 1D model lies on the source terms which is now multiply by β (respectively, $1-\beta$). We impose to preserve the same discrete form of the source terms. Such a choice is crucial to enforce the relevant asymptotic behavior of the scheme; namely the asymptotic preserving property.

After (3.58) and (3.59), the flux function involved in the Riemann solver has to satisfy:

$$\begin{aligned}
&\tilde{\mathcal{F}}^{\mathrm{HLLC}}_{L,R} = \alpha \tilde{\mathcal{F}}^{\mathrm{HLL}} + (1-\alpha)\mathcal{S}^{a}_{L,R},\\
&\mathcal{S}^{a}_{L,R} = \beta b_{L,R}\left(\mathcal{U}^{a}_{L,R} - \mathcal{U}_{L,R}\right),
\end{aligned}$$

where α is once again defined by (3.17) and

$$\mathcal{U} = {}^{t}\left(E, \frac{F_x}{c}, \frac{F_y}{c}\right) \quad \text{and} \quad \mathcal{F} = {}^{t}\left(F_x, cP_{xx}, cP_{xy}\right). \tag{4.3}$$

Following (3.54), the states $\mathcal{U}^{a}_{L,R}$ are given by

$$\mathcal{U}^{a}_{L,R} = \begin{pmatrix} a(T^{\star}_{L,R})^4 \\ 0 \\ 0 \end{pmatrix}, \tag{4.4}$$

where $T^{\star}_{L,R}$ is solution of the following equation (see (3.55)):

$$\rho C_v T^{\star}_{L,R} + (1-\alpha)a(T^{\star}_{L,R})^4 = \rho C_v T_{L,R} + (1-\alpha)\left(E_{L,R} - \frac{(F_x)_{L,R}}{b_{L,R}}\right). \tag{4.5}$$

As usual (see Harten *et al.* [14] and Toro [22] or the Equations (3.23)–(3.24)), we have set

$$\tilde{\mathcal{F}}^{\mathrm{HLL}} = \frac{1}{b_R - b_L}\left(b_R\mathcal{F}_L - b_L\mathcal{F}_R - b_L b_R(\mathcal{U}_L - \mathcal{U}_R)\right).$$

Now, we characterize the star region states $\mathcal{U}^{\star,\mathrm{HLLC}}_{L,R}$. To access such an issue, we involve the Rankine–Hugoniot relations, which reads:

$$b_{L,R}\left(\mathcal{U}^{\star,\mathrm{HLLC}}_{L,R} - \mathcal{U}_{L,R}\right) = \tilde{\mathcal{F}}^{\mathrm{HLLC}}_{L,R} - \mathcal{F}_{L,R}$$

to immediately deduce

$$\mathcal{U}^{\star,\mathrm{HLLC}}_{L,R} = \alpha\mathcal{U}^{\star,\mathrm{HLL}} + (1-\alpha)\mathcal{U}^{\star,a}_{L,R}, \tag{4.6}$$

where

$$\mathcal{U}^{\star,a}_{L,R} = \beta \mathcal{U}^{a}_{L,R} + (1-\beta)\mathcal{U}^{0}_{L,R},$$
$$\mathcal{U}^{0}_{L,R} = \mathcal{U}_{L,R} - \frac{1}{b_{L,R}}\mathcal{F}_{L,R}.$$

The state $\mathcal{U}^{\star,\mathrm{HLL}}$ is defined as the usual HLL star region state (see Harten *et al.* [14] and Toro [22] and Eq. (3.21) and (3.22)):

$$\mathcal{U}^{\star,\mathrm{HLL}} = \frac{1}{b_R - b_L}\left(b_R\mathcal{U}_R - b_L\mathcal{U}_L - (\mathcal{F}_R - \mathcal{F}_L)\right).$$

Now, the approximate Riemann solver is achieved as soon as the matter temperature $T^{\star,\mathrm{HLLC}}_{L,R}$ is defined. Once again, we enforce the same discretization of the source terms. Involving (3.61), we impose

$$\mathcal{S}^{T}_{L,R} = -\beta b_{L,R}(1-\alpha)\left(a(T^{\star}_{L,R})^4 - E^{0}_{L,R}\right),$$

which coincides with (3.61) detailed in the 1D model when multiplyed by β. Since we have

$$\mathcal{S}^{T}_{L,R} = b_{L,R}\rho C_v\left(T^{\star,\mathrm{HLLC}}_{L,R} - T_{L,R}\right),$$

we immediately deduce

$$\begin{aligned}\rho C_v T^{\star,\mathrm{HLLC}}_{L,R} &= \rho C_v T_{L,R} - \beta(1-\alpha)\left(a(T^{\star}_{L,R})^4 - E^{0}_{L,R}\right),\\ &= \beta\rho C_v T^{\star}_{L,R} + (1-\beta)\rho C_v T_{L,R}.\end{aligned} \tag{4.7}$$

Let us note that

$$\mathcal{S}^{T}_{L,R} = (1-\alpha)\mathcal{S}^{E,a}_{L,R}, \tag{4.8}$$

where $\mathcal{S}^{E,a}_{L,R}$ is the first component of $\mathcal{S}^{a}_{L,R}$. This remark will be useful when establishing the conservation of the approximate total energy.

Now, we turn establishing that the star states, involved in the approximate Riemann solver, remain in $\mathcal{A}$ while the matter temperature is positive.

Lemma 4.1. Assume $b_L < 0$ and $b_R > 0$. Let us assume that $\mathcal{U}^{0}_{L,R}$ are in $\mathcal{A}$. Then, the vectors $\mathcal{U}^{\star,\mathrm{HLLC}}_{L,R}$, defined by (4.6), belong in $\mathcal{A}$. In addition, the matter temperature is positive: $T^{\star,\mathrm{HLLC}}_{L,R} > 0$.

Let us emphasize that the assumption $\mathcal{U}^0_{L,R} \in \mathcal{A}$ turns out to be conditions to be satisfied by the velocities b_L and b_R. These conditions are nothing but the 2D extension of (3.44) and (3.45). They are specified in the following result:

Lemma 4.2. Let $\mathcal{U}$ be in $\mathcal{A}$ and, with $b \neq 0$, $\mathcal{U}^0$ be defined as follows:

$$\mathcal{U}^0 = \mathcal{U} - \frac{1}{b}\mathcal{F}.$$

Define $b^{\pm}$ by

$$\begin{aligned} b^{\pm}(\mathcal{U}) &= c\frac{f_x - f_x\chi_x - f_y\chi_y \pm \sqrt{\delta}}{1 - f_x^2 - f_y^2}, \\ \delta &= (f_x - f_x\chi_x - f_y\chi_y)^2 - (1 - f_x^2 - f_y^2)(f_x^2 - \chi_x^2 - \chi_y^2) > 0, \end{aligned} \tag{4.9}$$

where we have set

$$\begin{aligned} f_x &= F_x/(cE), \qquad & f_y &= F_y/(cE), \\ \chi_x &= P_{xx}/E, \qquad & \chi_y &= P_{xy}/E. \end{aligned} \tag{4.10}$$

Assume that

$$b \geq \max(b^+(\mathcal{U}), b^-(\mathcal{U})) \quad \text{or} \quad b \leqslant \min(b^+(\mathcal{U}), b^-(\mathcal{U})) \tag{4.11}$$

and

$$b^2 \geqslant cf_x b, \tag{4.12}$$

then $\mathcal{U}^0$ belongs to $\mathcal{A}$.

Before, we establish this lemma, let us emphasize the consequence implies by such a result. Indeed, the vectors $\mathcal{U}_{L,R}$ and $\mathcal{U}^0_{L,R}$ satisfy the assumptions stated Lemma 4.2. Then, we have $\mathcal{U}^0_{L,R}$ in $\mathcal{A}$ as soon as $b_{L,R}$ satisfies (4.11) and (4.12). Next, the assumptions of Lemma 4.1 are satisfied. First, we establish Lemma 4.2.

Proof. By definition, we have

$$\mathcal{U}^0 = \begin{pmatrix} E - F_x/b \\ F_x - c^2 P_{xx}/b \\ F_y - c^2 P_{xy}/b \end{pmatrix},$$

which must satisfy both positiveness and flux limitation properties. The positiveness is established as soon as we have

$$E - \frac{F_x}{b} = E\left(1 - \frac{c}{b} f_x\right) > 0.$$

This inequality is satisfied when involving (4.12). Now, we turn considering the flux limitation, which reads as follows:

$$\left(F_x - c^2\frac{P_{xx}}{b}\right)^2 + \left(F_y - c^2\frac{P_{xy}}{b}\right)^2 < c^2\left(E - \frac{F_x}{b}\right)^2.$$

Involving the notations (4.10), we rewrite

$$\left(\frac{b}{c}f_x - \chi_x\right)^2 + \left(\frac{b}{c}f_y - \chi_y\right)^2 < \left(\frac{b}{c} - f_x\right)^2.$$

After usual computations, we obtain

$$\left(1 - f_x^2 - f_y^2\right)\left(b - b^-\right)\left(b - b^+\right) > 0,$$

and the proof is completed. □

Now, we turn proving Lemma 4.1.

Proof. First, let us note that the assumption $\mathcal{U}^0_{L,R} \in \mathcal{A}$ implies $\mathcal{U}^{\star,\mathrm{HLL}} \in \mathcal{A}$. Indeed, we have

$$\mathcal{U}^{\star,\mathrm{HLL}} = \frac{b_R}{b_R - b_L}\mathcal{U}^0_R + \frac{-b_L}{b_R - b_L}\mathcal{U}^0_L.$$

Since $\mathcal{A}$ is a convex set, we immediately deduce that $\mathcal{U}^{\star,\mathrm{HLL}} \in \mathcal{A}$.

Now, involving (4.6) and the convex property of $\mathcal{A}$, we have just to prove that $\mathcal{U}^{\star,a}_{L,R} \in \mathcal{A}$ to ensure that $\mathcal{U}^{\star,\mathrm{HLLC}}_{L,R}$ belongs to $\mathcal{A}$. Let us recall that $\mathcal{U}^{\star,a}_{L,R} = \beta\mathcal{U}^a_{L,R} + (1-\beta)\mathcal{U}^0_{L,R}$. As a consequence, the result is established as soon as we have $\mathcal{U}^a_{L,R} \in \mathcal{A}$. When $\mathcal{U}^a_{L,R}$ being defined by (4.4), the result arises as soon as $T^\star_{L,R}$ is shown to be positive. Sine $T^\star_{L,R}$ is solution of (4.5), we can apply Lemma 3.3 and thus to obtain $T^\star_{L,R} > 0$. The proof is thus completed. □

We have describe an approximate Riemann solver corresponding to the system (4.1). The same analysis yields to an approximate Riemann solver but for the system (4.2). Both approximate Riemann solvers are now used to integrate a 2D numerical scheme on a Cartesian grid. To simplify, the mesh size Δx and Δy will be uniform. The time increment is evaluated according with the following CFL like conditions:

$$\begin{aligned}
&\frac{\Delta t}{\Delta x}\max_{i\in\mathbb{Z}}\left(|b_L^{x,i-\frac{1}{2}}|, b_R^{x,i+\frac{1}{2}}\right) \leqslant \frac{1}{2},\\
&\frac{\Delta t}{\Delta y}\max_{i\in\mathbb{Z}}\left(|b_L^{y,j-\frac{1}{2}}|, b_R^{y,j+\frac{1}{2}}\right) \leqslant \frac{1}{2},
\end{aligned} \tag{4.13}$$

where the wavespeeds are evaluated involving the exact 2D eigenvalues given by (2.4).

These velocities have to be restricted according to Lemma 4.1. The following formulas are proposed:

$$b_L^{x,i+\frac{1}{2}} = \min\left(0, cf_{x,i}^n, b^+(\mathcal{U}_{ij}^n), b^-(\mathcal{U}_{ij}^n), \lambda^-(\mathcal{U}_{ij}^n)\right), \tag{4.14}$$

$$b_R^{x,i-\frac{1}{2}} = \max\left(0, cf_{x,i}^n, b^+(\mathcal{U}_{ij}^n), b^-(\mathcal{U}_{ij}^n), \lambda^+(\mathcal{U}_{ij}^n)\right), \tag{4.15}$$

where $b^{\pm}$ are defined by (4.9). Concerning $b_{L,R}^{y,j+\frac{1}{2}}$, similar formulas have to be considered when reversing the role of f_x and f_y.

After computations, the scheme reads as follows:

$$\begin{aligned} E_{i,j}^{n+1} = E_{i,j}^n &- \frac{\Delta t}{\Delta x}\left(\left(\tilde{F}_{x,L}^{\mathrm{HLLC}}\right)_{i+\frac{1}{2},j} - \left(\tilde{F}_{x,R}^{\mathrm{HLLC}}\right)_{i-\frac{1}{2},j}\right) \\ &- \frac{\Delta t}{\Delta y}\left(\left(\tilde{F}_{y,L}^{\mathrm{HLLC}}\right)_{i,j+\frac{1}{2}} - \left(\tilde{F}_{y,R}^{\mathrm{HLLC}}\right)_{i,j-\frac{1}{2}}\right), \end{aligned} \tag{4.16a}$$

$$\begin{aligned} \frac{(F_x)_{i,j}^{n+1}}{c} = \frac{(F_x)_{i,j}^n}{c} &- \frac{\Delta t}{\Delta x} c\left(\left(\tilde{P}_{xx,L}^{\mathrm{HLLC}}\right)_{i+\frac{1}{2},j} - \left(\tilde{P}_{xx,R}^{\mathrm{HLLC}}\right)_{i-\frac{1}{2},j}\right) \\ &- \frac{\Delta t}{\Delta y} c\left(\left(\tilde{P}_{xy,L}^{\mathrm{HLLC}}\right)_{i,j+\frac{1}{2}} - \left(\tilde{P}_{xy,R}^{\mathrm{HLLC}}\right)_{i,j-\frac{1}{2}}\right), \end{aligned} \tag{4.16b}$$

$$\begin{aligned} \frac{(F_y)_{i,j}^{n+1}}{c} = \frac{(F_y)_{i,j}^n}{c} &- \frac{\Delta t}{\Delta x} c\left(\left(\tilde{P}_{xy,L}^{\mathrm{HLLC}}\right)_{i+\frac{1}{2},j} - \left(\tilde{P}_{xy,R}^{\mathrm{HLLC}}\right)_{i-\frac{1}{2},j}\right) \\ &- \frac{\Delta t}{\Delta y} c\left(\left(\tilde{P}_{yy,L}^{\mathrm{HLLC}}\right)_{i,j+\frac{1}{2}} - \left(\tilde{P}_{yy,R}^{\mathrm{HLLC}}\right)_{i,j-\frac{1}{2}}\right), \end{aligned} \tag{4.16c}$$

$$\begin{aligned} \rho C_v T_{i,j}^{n+1} = \rho C_v T_{i,j}^n &+ \frac{\Delta t}{\Delta x}\left(\left(\mathcal{S}_{x,L}^T\right)_{i+\frac{1}{2},j} - \left(\mathcal{S}_{x,R}^T\right)_{i-\frac{1}{2},j}\right) \\ &+ \frac{\Delta t}{\Delta y}\left(\left(\mathcal{S}_{y,L}^T\right)_{i,j+\frac{1}{2}} - \left(\mathcal{S}_{y,R}^T\right)_{i,j-\frac{1}{2}}\right). \end{aligned} \tag{4.16d}$$

Let us conclude when giving the main properties satisfied by the approximate solution.

Theorem 4.3. Let $\mathcal{U}_{i,j}^n$ be in $\mathcal{A}$ and $T_{i,j}^n$ be positive. Assume the CFL restriction (4.13) where the wavespeeds in each direction are restricted according to Lemma 4.1. Then, we have $\mathcal{U}_{i,j}^{n+1}$ in $\mathcal{A}$, $T_{i,j}^{n+1}$ positive and the total energy is conserved.

We omit the proof of the above result. Indeed, the proof is analogous to the proof of Theorem 3.5. Just, let us emphasize that $\mathcal{U}_{i,j}^{n+1} \in \mathcal{A}$ is a direct consequence of Lemma 4.1. Concerning the conservation of the total energy, the result is implied by the relation (4.8).

The last point, we develop concerns the asymptotic preserving property of the scheme. We do not detail the computations and the reader is referred to the section devoted to the 1D model. However, after introducing the rescaling based on the Knudsen number ϵ, the 2D version of Theorem 3.6 holds true:

Theorem 4.4. Assume that the wavespeeds are given by (4.14) and (4.15). With ϵ small, the diffusion limit behavior of the scheme (4.16) is as follows:

$$
\begin{aligned}
&E_{i,j}^n = a(T_{i,j}^n)^4,\\
&F_{i,j}^n = 0,\\
&\frac{(E+\rho C_v T)_{i,j}^{n+1} - (E+\rho C_v T)_{i,j}^n}{\Delta t}\\
&\quad = \frac{c}{3\Delta x^2}\left(\frac{1}{\sigma_{i+\frac{1}{2},j}}(E_{i+1,j}^n - E_{i,j}^n) + \frac{1}{\sigma_{i-\frac{1}{2},j}}(E_{i-1,j}^n - E_{i,j}^n)\right)\\
&\qquad + \frac{c}{3\Delta y^2}\left(\frac{1}{\sigma_{i,j+\frac{1}{2}}}(E_{i,j+1}^n - E_{i,j}^n) + \frac{1}{\sigma_{i,j-\frac{1}{2}}}(E_{i,j-1}^n - E_{i,j}^n)\right).
\end{aligned}
$$

5. NUMERICAL EXPERIMENTS

Now, we turn considering numerical applications to illustrate the interest of the present method in both one and two space dimensions.

Two main numerical aspects will be considered in this section. The first will be devoted to the influence of the numerical wavepeeds b_L and b_R, which enclose the Riemann problem in HLLC schemes. These wavespeeds will be taken either as in (3.66) and (3.67) or as $b_R = -b_L = c$ to enforce the maximal stability. The first choice will be denoted HLLC-var scheme and the second HLLC-c scheme.

The second aspect concerns the influence of the asymptotic preserving modification of the HLLC scheme introduced in 3. The scheme with or without this modification will be denoted AP-HLLC or HLLC scheme, leading to four variants (HLLC-c, HLLC-var, AP-HLLC-c, AP-HLLC-var) that will be compared. All the numerical experiments are performed using an Intel Pentium Centrino with 1.7 GHz clock frequency. The 2D

computations given in Sect. 5.4 need about one minute CPU time to be completed.

5.1. Marshak Wave

The fisrt problem comes from [24]. This test problem consists of a slab of material with opacity $\sigma = 100$, and $\rho C_v = 10^{-4}$, extending from $x = 0$ to $x = 0.1$. A temperature source with $T = 1000$, on the left side generates a thermal wave into the initialy cold medium, which is at equilibrium with an initial temperature $T = 300$. In this test case we use a mesh with ten cells.

Comparison of M_1 solution computed using the AP-HLLC-var scheme with M_1 solution computed using the HLLC-var scheme and a reference solution obtained by full transport calculation (see [24]) is shown in Fig. 5 at three times ($t_1 = 1.33 * 10^{-9}$, $t_2 = 1.33 * 10^{-8}$, $t_3 = 1.33 * 10^{-7}$).

In this computation the cell size $\Delta x = 0.01$ does not sample the mean free path $\lambda = 1/\sigma = 0.01$. As we expected the M_1 solution computed using the HLLC-c scheme clearly overestimates the radiative energy, mostly in early times whereas the M_1 solution computed using the AP-HLLC-var scheme gives a much better agreement with the reference solution.

The influence of the choice of the numerical wavespeeds b_L and b_R is shown in Fig. 6. We compare, on the same test case, at time t_3, the four variants of our scheme (HLLC-c, HLLE-var, AP-HLLC-c,

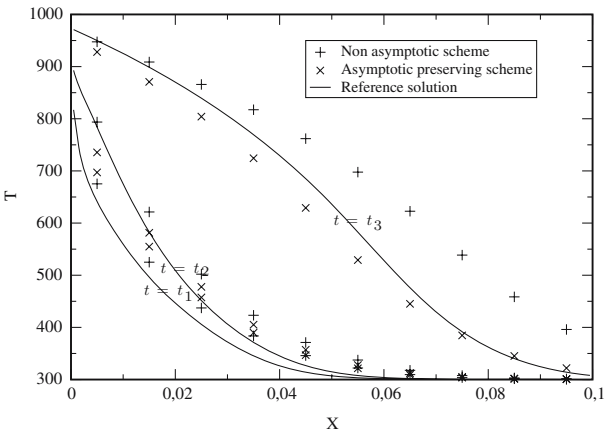

Fig. 5. Radiation temperature for $t_1 = 1.33 * 10^{-9}$, $t_2 = 1.33 * 10^{-8}$, and $t_3 = 1.33 * 10^{-7}$. Results from the HLLC-var and AP-HLLC-var schemes are compared with the kinetic reference solution obtained in [24].

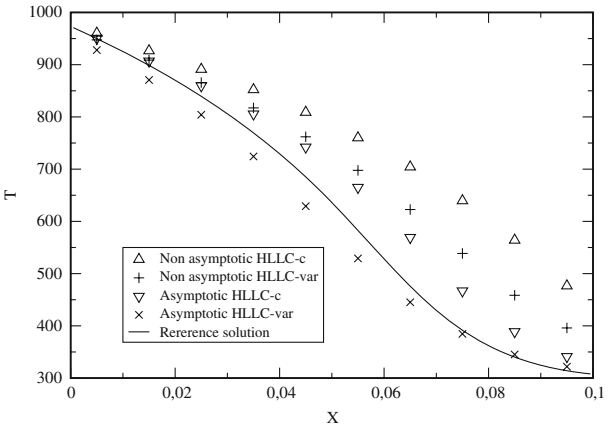

Fig. 6. Radiation temperature for $t = 1.33 * 10^{-7}$ obtained thanks to the HLLC-c and HLLC-var, AP-HLLC-c and AP-HLLC-var are compared from the X-Skinetic reference solution obtained in [24].

AP-HLLC-var) with the reference solution. Obviously, taking too large numerical wavespeeds ($b_L = -c$ and $b_R = +c$) brings a too large amount of numerical diffusion. Improving the HLLC-c scheme by using sharper wavespeeds estimates or by using the asymptotic preserving modification gives roughly the same improvement of accuracy and, as expected, the best result is obtained with the AP-HLLC-var variant combining the two modifications.

5.2. Opaque Materials

We now examine two problems, which involve opaque materials and where we are able to compute the exact steady state solution of the equilibrium diffusium model.

The first problem comes from [11]. This test problem consists of a slab of material with opacity $\sigma = 100$ and $\rho C_v = 1$, extending from $x = 0$ to $x = 10$. A temperature source with $T = 1$, on the left side generates a thermal wave into the initially cold slab, which is at equilibrium and has an initial temperature of $T = 10^{-3}$. A vacuum boundary condition is imposed at $x = 10$. The units are chosen such that $c = a = 1$. Two simulations are performed with two different meshes of, respectively, 20 and 100 cells, so that the mean free path is not resolved.

Figure 7 shows the radiation temperature at steady state for a simulation run with the AP-HLLC-var scheme on the two different meshes.

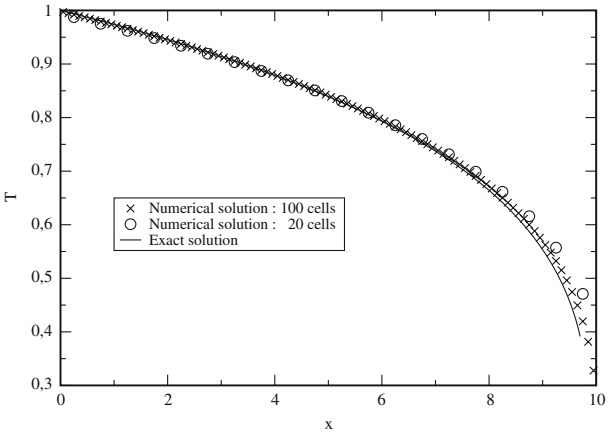

Fig. 7. Steady radiation temperature obtained thanks to the HLLC-var and AP-HLLC-var schemes on two different meshes are compared with the exact solution. A material opacity $\sigma = 100$ is used.

The two computations produced almost identical results, both very closed to the exact steady solution of the equilibrium diffusion model.

For the second problem we keep the same parameters except the opacity. We introduce a low-opacity region with $\sigma = 100$ which extend from $x = 0$ to $x = 5$ and a high-opacity region with $\sigma = 200$ which extend from $x = 5$ to $x = 10$.

Figure 8 shows the radiation temperature for a simulation run with the AP-HLLC-var scheme on the two meshes. A good agreement with the exact solution of the equilibrium diffusion model can be found again.

Figure 9 shows the influence of the asymptotic preserving modification. We use here the finest mesh with 100 cells. The HLLC-var scheme and the AP-HLLC-var are compared. Again, the solution of HLLC-var scheme is far away from the exact solution. On the other hand, in both cases the boundary conditions are satisfied. The upwind HLLC-var scheme is too dissipative and is not able to see the transition area between the low-and high-opacity regions.

5.3. Hybrid Case: Transparent to Opaque Transition

For this case, an hybrid problem for checking the transition between transparent and opaque regions is considered. This test problem consists of a slab with a region of transparent material with opacity $\sigma = 0.1$, extending from $x = 0$ to $x = 5$ and a region of opaque material with $\sigma =$

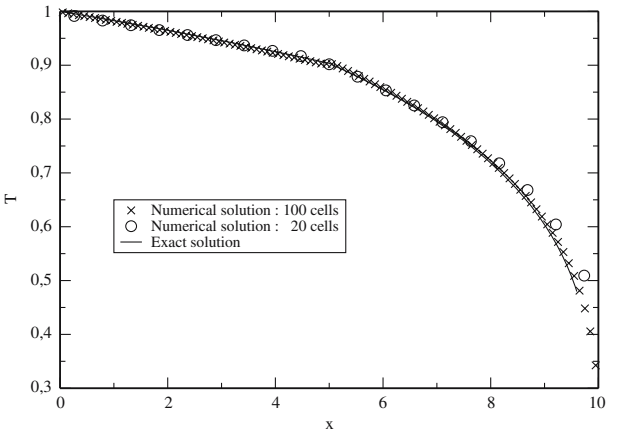

Fig. 8. Steady radiation temperature obtained thanks to the HLLC-var and AP-HLLC-var schemes on two different meshes are compared with the exact solution. The material opacities $\sigma = 100$ for $x < 5$ and $\sigma = 200$ for $x > 5$ are used.

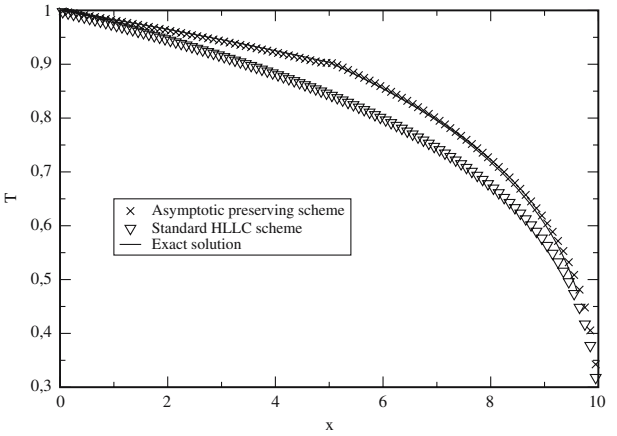

Fig. 9. Steady radiation temperature obtained thanks to the HLLC-var and AP-HLLC-var schemes are compared with the exact solution. The material opacities $\sigma = 100$ for $x < 5$ and $\sigma = 200$ for $x > 5$ are used.

100, extending from $x = 5$ to $x = 10$. A temperature source with $T = 1$, on theleft side generates a thermal wave into the initially cold medium, which is at equilibrium and has an initial temperature of $T = 10^{-3}$. A vacuum boundary condition is imposed at $x = 10$. The units are chosen such that $c = a = 1$.

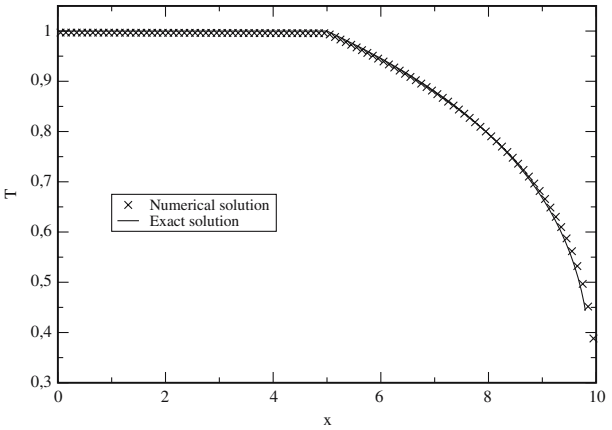

Fig. 10. Steady radiation temperature obtained thanks to the HLLC-var and AP-HLLC-var are compared with the exact solution. The material opacities $\sigma = 0.1$ for $x < 5$ and $\sigma = 100$ for $x > 5$ are used.

Figure 10 shows the steady radiation temperature obtained from the AP-HLLC-var scheme, which was run with 100 cells compared with the exact steady solution of the equilibrium diffusion model. A good agreement can be observed. The AP-HLLC-var scheme proves to be able to handle the wave crossing the interface between the transparent and opaque regions.

This conclusion is enforced by the Fig. 11 where the material and radiative temperatures are plotted at five different times. The last time is taken sufficiently high to be close to the steady state. The phenomena in the opaque material is a Marshak wave except of a small preheating area where the material temperature is not the same as the radiative temperature. In this area, the transport is dominant, and the diffusion assumption is not verified.

5.4. Two Dimensionnal Case

The fourth problem is a two dimensional problem developed to focus on purely two dimensional effects. A Cartesian mesh made of 80×40 cells is used. In this problem, we consider free streaming beam adjacent to some section of dense, opaque material. The opaque region extends from $x = 0$ to $x = 0.5$ and from $y = 0$ to $y = 0.5$. Outside, we consider a transparent region which extends from $x = 0$ to $x = 2$ and from $y = 0$ to $y = 2$. In the dense material $\rho C_v = 8.6 \times 10^4$, $\sigma = 2 \times 10^5$. The outside material is purely transparent, i.e. $\sigma = 0$. The geometry is summarized on Fig. 12.

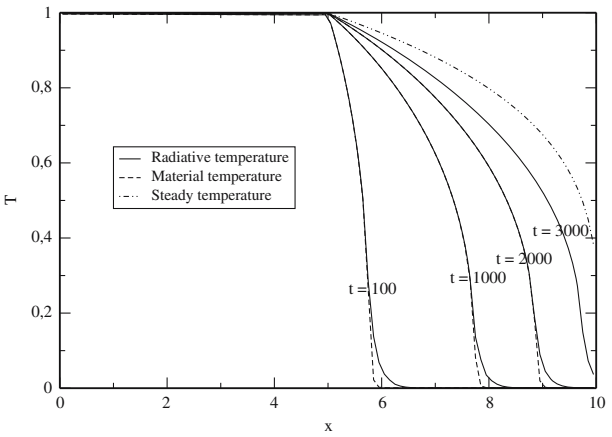

Fig. 11. Radiation and material temperatures for $t = 100$, $t = 1000$, $t = 2000$, $t = 3000$, and for the steady state are obtained thanks to the AP-HLLC-var scheme.

A radiative temperature $T = 5,802,000$ $(=5keV)$ is applied on the left-side of the transparent material from $y = 0.5$ to $y = 1$ (see Fig. 12). Vacuum boundary condition are applied at all other boundaries. The initial temperature is $T = 50,000$ in the dense material and $T = 300$ elsewhere. All the computations are run on a cartesian mesh of 80×40 cells and the parameter β, introduced in (4.1), is defined as follows:

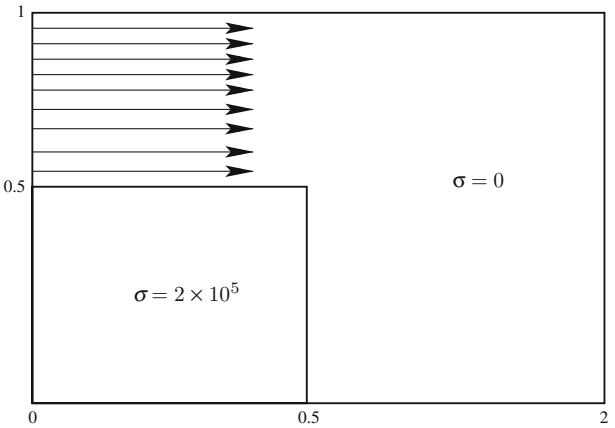

Fig. 12. Geometry for the two dimensional case.

$$\beta = \begin{cases} \left(\frac{\boldsymbol{f}.\mathbf{n}}{f}\right)^2, & \text{if } f \neq 0, \\ \frac{1}{2}, & \text{if } f = 0, \end{cases}$$

where $\mathbf{n}$ is the outward normal of the cell interface. The simulation is stopped at the time $t = 5 \times 10^{-8}$.

The expected solution is very simple. In the upper part, from $y = 0.5$ to $y = 1$ the solution is a translation of the left boundary condition, the radiative temperature is $T = 58,02,000$ and the photons remains in free streaming ($f \approx 1$). In the lower part, from $y = 0$ to $y = 0.5$ the solution is constant in time because there is no photons which are entering in this area. The line $y = 0.5$ is a stanionary contact discontinuity for the M_1 system.

In the Figs. (13–15), we examine the ability of the various variants of our scheme to capture this solution. The Fig. 13 shows the radiative temperature, the Fig. 14 shows the material temperature in the obstacle, and the Fig. 15 shows the anisotropy factor f, for each variant of the scheme.

Figure 13 shows the influence of the numerical wavespeeds b_L and b_R. We compare the -c and the -var versions of both HLLC and AP-HLLC schemes. The numerical dissipation of the -c variant, espacially in the y-direction, does not allow this schemes to preserve the contact discontinuity and we observe a lot of photons penetrating the lower part of the domain. On the other hand the contact discontinuity is nearly exactly preserved in the -var versions of the two schemes. More precisely, at a point $y = 0.5,\ x > 0.5$ on a cell interface in y-direction, in the "left" cell

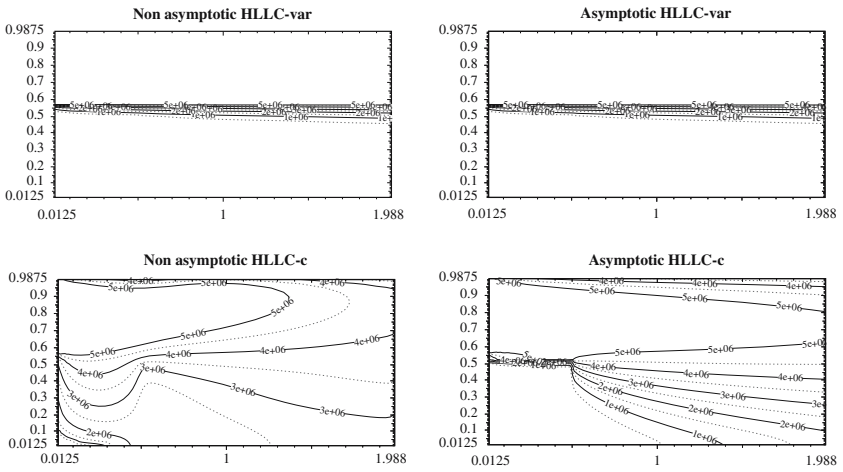

Fig. 13. Radiation temperature at $t = 5 * 10^{-8}$ obtained thanks to the HLLC-c and HLLC-var, AP-HLLC-c and AP-HLLC-var schemes.

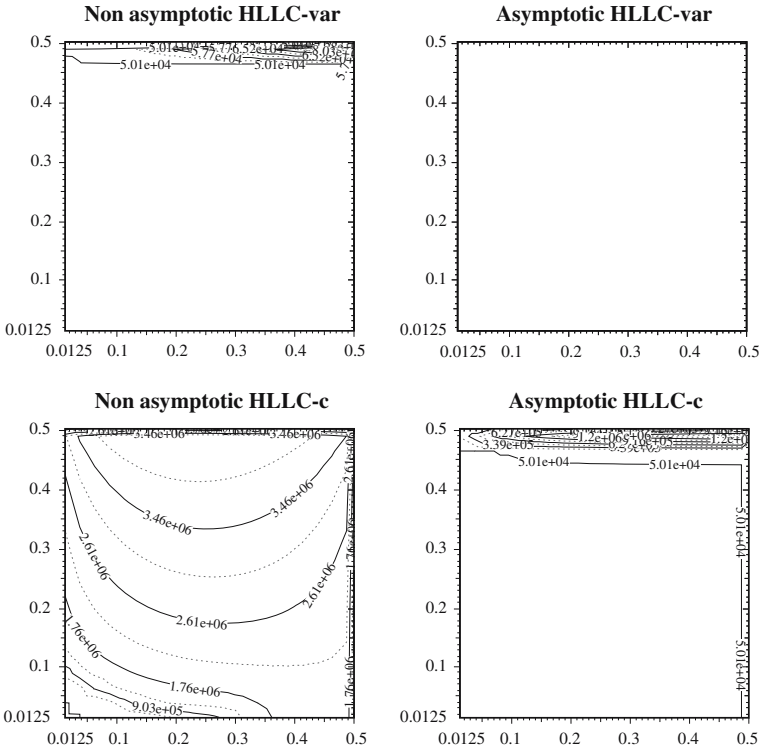

Fig. 14. Material temperature at $t = 5 * 10^{-8}$ obtained thanks to the HLLC-c and HLLC-var, AP-HLLC-c and AP-HLLC-var schemes.

$f_x = f_y \approx 0$ and in the "right" cell $f_x \approx 1$, $f_y \approx 0$, and for the -var scheme $b_L = -c/\sqrt{3}$, $b_R \approx 0$ (3.66) and (3.67); the -c version (and every scheme using symmetric wavespeeds, $b_L = -b_R$) introduces there a numerical diffusion responsible for (nonphysical) penetration of photons in the lower part of the domain. The necessity of using sharp numerical wavespeeds estimates is clearly proved.

Figure 14 shows the improvement brought by the asymptotic preserving modification. Indeed for both HLLC-c and HLLC-var schemes the heating of the opaque medium is much more important without the asymptotic preserving modification. When using the HLLC-c scheme a large amount of photons penetrates the the lower opaque region (wrong wavespeeds), which is too much heated (wrong behavior in the diffusion regime), and the material temperature raises and the medium emits energetic photons which perturb the solution in transparent regions.

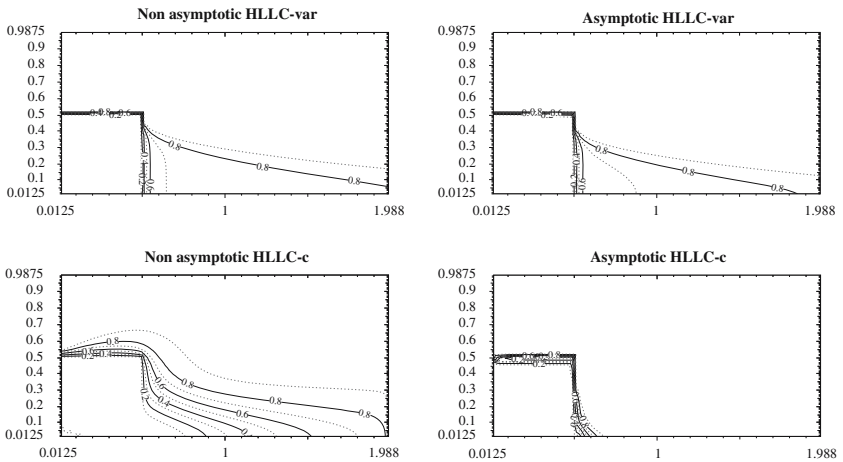

Fig. 15. Anisotropy factor at $t = 5 * 10^{-8}$ obtained thanks to the the HLLC-c and HLLC-var, AP-HLLC-c and AP-HLLC-var schemes.

Finally, it appears that we need to use sharp numerical wavespeeds estimates and asymptotic preserving modification, i.e. the AP-HLLC-var scheme, to capture with accuracy the solution of this problem.

6. CONCLUSION

In the present work, we have exhibited a new numerical method to approximate the solutions of the M_1 model of radiative transfer. This procedure is based on predictor-corrector scheme and it uses an HLLC scheme. A particular attention has been payed to satisfy the positiveness of the energy and the flux limitation property. As a consequence, the scheme has been proved to be robust. In addition, we have established the asymptotic preserving property of the scheme. The accuracy of the method has been ensured when considering approximate Riemann solver with a characteristic cone which is not necessary symmetric. Such an independent choice of the extreme approximate wavespeeds gives accurate numerical results into the simulations. Indeed, when simulations involving a shadow cone are performed, a scheme using an approximate Riemann solver with a symmetric characteristic cone involves very large numerical diffusion while our proposed scheme produces results in very good agreement with the physics.

REFERENCES

1. Audit, E., Charrier, P., Chièze, J.-P., and Dubroca, B. (2002). A radiation hydrodynamics scheme valid from the transport to the diffusion limit, preprint astro-ph 0206281.
2. Batten, P., Clarke, N., Lambert, C., and Causon, D. M. (1997). On the choice of wavespeeds for the HLLC Riemann solver. *SIAM J. Sci. Comput.* **18** (6), 1553–1570.
3. Berthon, C. Numerical approximations of the 10-moment Gaussian closure. *Math. Comp.* Posted on June 6, 2006, PII S 0025–5718(06)01860-6 (to appear in print).
4. Berthon, C., Charrier, P., and Dubroca, B. An asymptotic preserving relaxation scheme for a moment model of the radiative transfer, C. R. Acad. Sci. Paris, Ser. I, submitted.
5. Bouchut, F. (2004). Nonlinear Stability of Finite Volume Methods for Hyperbolic Conservation Laws, and Well-Balanced Schemes for sources. Frontiers in Mathematics series, Birkhäuser.
6. Buet, C., and Cordier, S. (2004). Asymptotic Preserving Scheme and Numerical Methods for Radiative Hydrodynamic Models. 951–956 *C. R. Acad. Sci.* Paris, Tome 338, Série I.
7. Buet, C., and Després, B. (2004) Asymptotic analysis of fluid models for the coupling of radiation and hydrodynamics. *J. Quant. Spectrosc. Radiat. Transf.* **85** (3–4), 385–418.
8. Buet, C., and Després B. (2006). Asymptotic preserving and positive schemes for radiation hydrodynamics, *J. Comput. Phys*. **215**, 717–740.
9. Charrier, P., Dubroca, B., Duffa G., and Turpault, R. (2003). Multigroup model for radiating flows during atmospheric hypersonic re-entry. *Proceedings of International Workshop on Radiation of High Temperature Gases in Atmospheric Entry*, pp. 103–110. Lisbonne, Portugal.
10. Dubroca, B., Feugeas, J.-L. (1999). Hiérarchie de Modéles Aux Moments Pour le Transfert Radiatif. Série I. pp. 915–920. *C. R. Acad. Sci.* Paris, Tome 329.
11. Gentile, N. A. (2001). Implicit Monte-carlo diffusion-an acceleration method for Monte Carlo time-dependent radiative transfer simulations. *J. Comput. Phys.* **172**, 543–571.
12. Godlewsky, E., and Raviart, P.A. (1995). Hyperbolic Systems of Conservations Laws, Applied Mathematical Sciences, Vol 118, Springer Berlin.
13. Gosse, L., and Toscani, G. (2002). Asymptotic-preserving well-balanced scheme for the hyperbolic heat equations. pp. 337–342. *C. R. Acad. Sci.* Paris, tome 334, Série I.
14. Harten, A., Lax, P.D., and Van Leer, B. (1983). On upstream differencing and Godunov-type schemes for hyperbolic conservation laws. *SIAM Rev.* **25**(1) 35–61.
15. Ingram, D.M., Causon, D.M., and Mingham, C.G. (2003). Developments in Cartesian cut cell methods. *Math. Comput. Simulat.* **61**, 561–572.
16. Jin, S., and Xin, Z. (1995). The relaxation scheme for systems of conservation laws in arbitrary space dimension. *Comm. Pure Appl. Math.* **45**, 235–276.
17. Levermore, C. D. (1996). Moment closure hierarchies for kinetic theory. *J. Stati. Phys.* **83**, 1021–1065.
18. Mihalas D., and Mihalas, G. W. (1984). *Foundation of Radiation Hydrodynamics*, Oxford University Press, Oxford.
19. Pomraning, G.C. (1973). The Equations of Radiation Hydrodynamics, Sciences Application, Pergamon Press, Oxford.
20. Ripoll, J.-F. (2004). An averaged formulation of the M1 radiation model with presumed probability density function for turbulent flows. *J. Quant. Spectrosc. Radiat. Trans.* **83**(3–4), 493–517.
21. Ripoll, J.-F., Dubroca, B., and Audit, E. (2002). A factored operator method for solving coupled radiation-hydrodynamics models. *Trans. Theory. Stat. Phys*. **31**, 531–557.
22. Toro, E. F. (1999). Riemann solvers and numerical methods for fluid dynamics. A practical introduction, 2nd edn. Springer-Verlag, Berlin.

23. Toro, E. F., Spruce, M., and Spear, W. (1994). Restoration of the contact surface in the HLL Riemann solver. *Shock waves*, **4**, 25–34.
24. Turpault, R. (2002). Numerical Solution of Radiative Transfer Equation with Finite Volumes. *Proceedings of Finite Volume for Complex Applications III,* pp. 695–702, France.
25. Turpault, R. (2005). A consistent multigroup model for radiative transfer and its underlying mean opacity. *J. Quant. Spectrosc. Radiat. Transfer* **94**, 357–371.